

On Oceanic Rogue Waves

FRANCESCO FEDELE*

School of Civil and Environmental Engineering, School of Electrical and Computer Engineering, Georgia Institute of Technology, Atlanta, GA, USA.

ABSTRACT

We propose a new conceptual framework for the prediction of rogue waves and third-order space-time extremes of wind seas that relies on the Tayfun (1980) and Janssen (2009) models coupled with Adler-Taylor (2009) theory on the Euler characteristics of random fields. As a specific application of this framework, extreme statistics of the 2007 Andrea rogue wave event are examined and verified with estimates from European Reanalysis (ERA)-interim data. In particular, the effects of nonlinear wave-wave interactions and space-time variability of the wave field are considered. A refinement of Janssen's (2003) theory suggests that in realistic oceanic seas characterized by short-crested multidirectional waves, homogeneous and Gaussian initial conditions become irrelevant as the wave field adjusts to a non-Gaussian state dominated by bound nonlinearities over time scales $t \gg t_c \approx 0.13T_0/\nu\sigma_\theta$, where T_0 , ν and σ_θ denote mean wave period, spectral bandwidth and angular spreading of dominant waves. For the Andrea storm, ERA-interim predictions yield $t_c/T_0 \sim O(1)$ indicating that quasi-resonant interactions are negligible. Further, the mean maximum sea surface height expected over the Ekofisk platform's area is higher than that expected at a fixed point within the same area. However, both of these statistics underestimate the actual crest height $h_{obs} \sim 1.63H_s$ observed at a point near the Ekofisk site, where H_s is the significant wave height. To explain the nature of such extreme, we account for both skewness and kurtosis effects and consider the threshold h_q exceeded with probability q by the maximum surface height of a sea state over an area in time. We find that h_{obs} nearly coincides with the threshold $h_{1/1000} \sim 1.62H_s$ estimated at a point for a typical 3-hour sea state, suggesting that the Andrea rogue wave is likely to be a rare occurrence in quasi-Gaussian seas.

1. Introduction

Rogue waves are unusually large-amplitude surface waves that appear from nowhere in the open ocean. Evidences that such extremes can occur in nature are provided by the Draupner and Andrea events. In particular, the Andrea rogue wave was measured just past 00 UTC on November 9 2007 by a LASAR system mounted on the Ekofisk platform in the North Sea in a water depth of $d = 74$ m (Magnusson and Donelan 2013). The Andrea wave has similar features of the Draupner freak wave measured by Statoil at a nearby platform ($d = 70$ m) in January 1995 (Haver 2001). Denoting the standard deviation of surface elevations by σ , the Andrea wave occurred during a sea state with significant wave height $H_s = 4\sigma = 9.2$ m, mean period $T_0 = 13.2$ s and wavelength $L_0 = 220$ m. The crest height is $h = 15$ m ($h/H_s = 1.63$) and the crest-to-trough height $H = 21.1$ m ($H/H_s = 2.3$) (Magnusson and Donelan 2013). The Draupner wave occurred during a 5-hour sea state with significant wave height $H_s = 4\sigma = 11.9$ m, mean period $T_0 = 13.1$ s and wavelength $L_0 = 250$ m.

The crest height is $h = 18.5$ m ($h/H_s = 1.55$) and the crest-to-trough height $H = 25.6$ m ($H/H_s = 2.15$) (Haver 2004; Magnusson and Donelan 2013). In the last decade, the properties of the Draupner and Andrea waves have been extensively studied (Dysthe et al. 2008; Osborne 2010; Magnusson and Donelan 2013; Bitner-Gregersen et al. 2014; Dias et al. 2015) and references therein). Several physical mechanisms have been proposed to explain the occurrence of such giant waves (Kharif and Pelinovsky 2003), including the two competing hypotheses of nonlinear focusing due to third-order quasi-resonant wave-wave interactions (Janssen (2003)), and purely dispersive focusing of second-order waves (Fedele and Tayfun 2009; Fedele 2008).

For instance, recent studies propose the hypothesis that the Draupner wave occurred in crossing seas (see e.g. Onorato et al. (2010)). These suggest that angles lying in the range $\sim 10^\circ - 30^\circ$ between two dominant sea directions are likely to lead to rogue-wave occurrences induced by quasi-resonant wave-wave interactions. However, Adcock et al. (2011) reported that the hindcast from the European Centre for Medium-Range Weather Forecasts shows swell waves propagating at approximately 80° to the wind

*Corresponding author address: Georgia Institute of Technology
Atlanta, GA 30332, USA.
E-mail: fedele@gatech.edu

sea. Adcock et al. (2011) also argued that the Draupner wave occurred due to the crossing of two almost orthogonal wave groups in accord with second-order theory. This would explain the set-up observed under the large wave (Walker et al. 2004) instead of the second-order set-down normally expected (Longuet-Higgins and Stewart 1964). However, there is no evidence of significant swell components nearby the platform as clearly seen from Fig. 2 in Adcock et al. (2011) and Fig. 1 here, which shows the ERA-interim wave directional spectrum at the Draupner site. Further, in accord with Boccotti's (2000) quasi-determinism (QD) theory the probability that two different wave groups cross at the same point at the apex of their development is much smaller than the probability that one of the two groups focuses at the same point. One can also argue that reflection and diffraction from the platform may cause the observed set-up. However, the Draupner measurements were made from a bridge connecting two space frame structures. The structural members are relatively small, likely a meter in diameter. The preceding greatly lessens the chances for platform interference from spray, reflections or diffractions. Clearly, the Draupner wave appears fundamentally different from a typical expected extreme wave because of the observed set-up of the mean sea level (MSL) below the large crest. However, the estimation of the MSL from measurements is ill-defined and thus may be not robust. Indeed, we note that Walker et al. (2004) estimated the mean sea level by low-pass filtering the measured time series of the wave surface with frequency cutoff $f_c \sim f_p/2$, where f_p is the dominant frequency. Clearly, the mean surface and wave fluctuations are nonlinearly coupled and feed energetically into each other. As a result, the low-pass filtered mean surface is a mix of the two components. If the time series is not long enough for a statistically significant estimation of wave-wave interactions, the observed set-up could be the manifestation of the large crest segment that extends above the adjacent lower crests. In this work, we will not dwell on the Draupner wave. This calls for further studies and numerical simulations of the sea state in which it occurred to clarify the physics and robustness of the observed set-up below the large crest. These issues are secondary and are beyond the scope of this paper. Indeed, we will capitalize on recent numerical simulations of the Andrea rogue wave (Bitner-Grøgersen et al. 2014; Dias et al. 2015) in order to study the statistical properties and space-time extremes of the sea state in which it occurred.

Other studies propose third-order quasi-resonant interactions and associated modulational instabilities as mechanisms for rogue wave formation (e.g. Janssen (2003); Osborne (2010)). Such nonlinear effects cause the statistics of weakly nonlinear gravity waves to significantly differ from the Gaussian structure of linear seas, especially in long-crested, or unidirectional seas (Janssen (2003); Fedele (2008); Onorato et al. (2009); Shemer and Sergeeva

(2009); Toffoli et al. (2010); Fedele et al. (2010)). The relative importance of such nonlinearities and the increased occurrence of large waves can be measured by the excess kurtosis

$$\lambda_{40} = \frac{\langle \eta^4 \rangle}{\langle \eta^2 \rangle^2} - 3, \quad (1)$$

of the mean-zero surface elevation η , where brackets denote statistical average. This integral statistic is defined by Janssen (2003) as $C_4 = \lambda_{40}/3$. In general, $C_4 = C_4^d + C_4^b$ and it comprises a dynamic component C_4^d due to nonlinear wave-wave interactions (Janssen (2003)) and a bound contribution C_4^b induced by the characteristic crest-trough asymmetry of ocean waves (Tayfun (1980); Tayfun and Lo (1990); Tayfun and Fedele (2007); Fedele and Tayfun (2009); Fedele (2008); Janssen and Bidlot (2009)). For deep-water long-crested seas with a Gaussian-shaped spectrum and within the framework of the higher order compact Zakharov (cDZ) equation (Dyachenko and Zakharov (2011)), Fedele (2014) showed that, correct to $O(v^2)$ in spectral bandwidth, the dynamic excess kurtosis monotonically increases in time toward the asymptotic value

$$C_{4,cDZ}^d = C_{4,NLS}^d \left(1 - \frac{4\sqrt{3} + \pi}{8\pi} v^2 \right) \approx C_{4,NLS}^d (1 - 0.40v^2),$$

where

$$C_{4,NLS}^d = BFI^2 \frac{\pi}{3\sqrt{3}} \quad (2)$$

is the dynamic excess kurtosis of unidirectional narrowband waves in deep water in accord with the one-dimensional (1-D) nonlinear Schrödinger (NLS) equation (Mori and Janssen (2006)). Note that Eq. (2) is also valid for the Dysthe (1979) equation as the associated asymmetric spectral broadening is not captured by the assumed symmetric Gaussian spectrum. The Benjamin-Feir index $BFI = \sqrt{2}\mu/v$, with μ denoting an integral measure of wave steepness defined later in Eq. (20) and the spectral bandwidth v is given in Eq. (21). Clearly, $C_{4,cDZ}^d$ is smaller than $C_{4,NLS}^d$, especially as the spectral bandwidth widens. This is consistent with the result that in accord with cDZ the linear growth rate of a subharmonic perturbation reduces with respect to the NLS counterpart for waves with broader spectra. Indeed, for fixed wave steepness, the initial-stage growth of instabilities away from a Stokes wave is attenuated as the spectral bandwidth increases (Alber (1978); Crawford et al. (1981)). The late-stage evolution of modulation instability leads to breathers that can cause large waves (Peregrine 1983; Osborne et al. 2000; Ankiewicz et al. 2009), especially in unidirectional waves. Indeed, in this case energy is "trapped" as in a long waveguide. For small wave steepness and negligible dissipation, quasi-resonant interactions are effective in reshaping the wave spectrum, inducing larger breathers via nonlinear focusing before breaking occurs (Shemer and Sergeeva

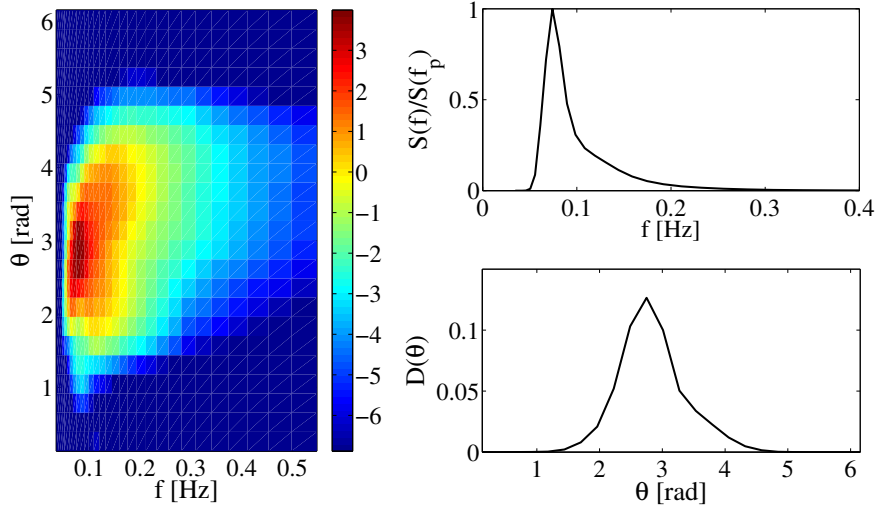


FIG. 1. Draupner storm: ERA-interim (left) directional spectrum (log scale) at the Draupner site (58.2° N, 2.5° E) at the time of maximum development of the storm (Jan 2nd 1995 00:00 UTC) and (top-right) wave frequency spectrum $S(f)/S(f_p)$ and (bottom-right) angular dispersion $\sigma^2 D(\theta) = \int S(f, \theta) df$, where σ is the standard deviation of surface elevations and f_p the dominant frequency. Direction $\theta = 0$ means going to the north and $\theta = \pi/2$ to the east (Oceanographic convention).

(2009); Onorato et al. (2009); Chabchoub et al. (2011, 2012)). Shemer and Alperovich (2013) pointed out that wave breaking is inevitable for $\mu > 0.1$, and breathers can be observed experimentally only at sufficiently small values of wave steepness ($\sim 0.01 - 0.09$) (Chabchoub et al. (2011, 2012), see also Shemer and Liberzon (2014)). Further, they also noted that 'breather does not breath' and its amplification is smaller than that predicted by the NLS, in accord with the numerical studies of the Euler equations (Slunyaev and Shrira (2013); Slunyaev et al. (2013)). However, typical oceanic wind seas are not 1-D but short-crested multidirectional wave fields. Hence, nonlinear focusing due to modulational effects is diminished since energy can spread directionally (Onorato et al. (2009); Toffoli et al. (2010)).

The sea state of the Andrea wave was short-crested (see Fig. 2), and modulation instabilities may have played an insignificant role in the wave growth (Alber 1978; Crawford et al. 1981). Further, the actual water depth to wavelength ratio, namely $d/L_0 \sim 0.3$, suggests that waves were in transitional regime where modulation instabilities, if any, are further attenuated (see, e.g. Toffoli et al. (2009)). Recently, Tayfun (2008) arrived at similar conclusions based on the analysis of data from the North Sea. His results indicate that large time waves (measured at a given point) result from the constructive interference (focusing) of elementary waves with random amplitudes and phases enhanced by second-order non-resonant interactions. Further, the surface statistics follow the Tayfun (1980) distribution in agreement with observations (Tayfun and Fedele (2007); Fedele (2008); Tayfun (2008); Fedele and Tayfun

(2009)). This is confirmed by a recent data quality control and statistical analysis by Christou and Ewans (2014) of single-point measurements from fixed sensors mounted on offshore platforms, the majority of which were recorded in the North Sea. The analysis of an ensemble of 122 million individual waves revealed 3649 rogue events, concluding that rogue waves observed at a point in time are merely rare events induced by dispersive focusing.

More recent studies on the statistics of extreme ocean waves provide both theoretical and experimental evidences that the expected maximum sea surface height over an area in time (space-time extreme) is larger than that expected at a fixed point (time extreme), especially in short-crested multidirectional seas (Forristall (2011, 2015); Fedele (2012); Fedele et al. (2013); Barbariol et al. (2014)). The occurrence of an extreme in Gaussian fields is analogous to that of a big wave that a surfer searches and eventually finds (Baxevani and Rychlik (2006)). If the surfer searches a large area, his chances of encountering the largest crest obviously increase. Indeed, a large number of radar signatures of likely rogue waves have been identified from satellite data in the context of the MaxWave project (Rosenthal and Lehner 2008). However, the relation between space-time extremes and rogue waves is still unclear.

The preceding review provides the principal motivation for introducing the theory of stochastic space-time extremes and applying it to study the space-time properties of sea states in which rogue waves occur. In this work, we only focus on the Andrea rogue event as the Draupner wave requires further studies on the observed

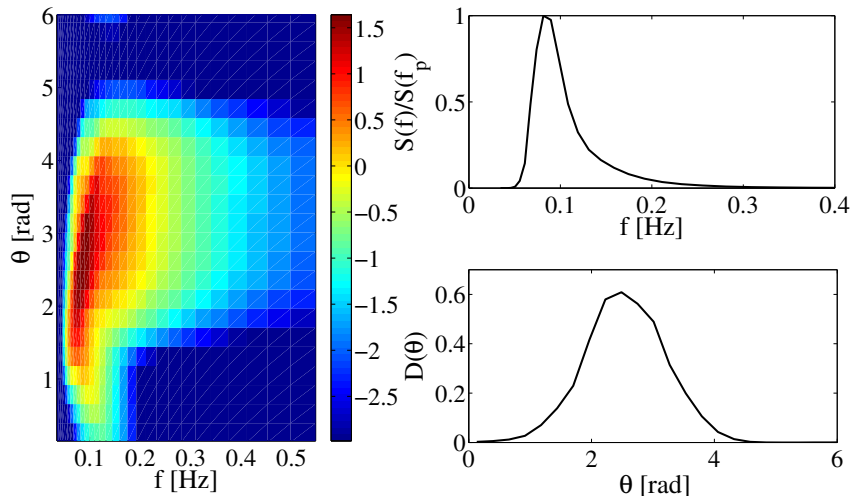


FIG. 2. Andrea storm: ERA-interim (left) directional spectrum (log scale) at the Ekofisk site (56.3° N, 3° E) at about the time of the Andrea wave event (Nov 9th 2007, 00:00 UTC) and (top-right) wave frequency spectrum $S(f)/S(f_p)$ and (bottom-right) angular dispersion $\sigma^2 D(\theta) = \int S(f, \theta) df$, where σ is the standard deviation of surface elevations and f_p the dominant frequency. Direction $\theta = 0$ means going to the north and $\theta = \pi/2$ to the east (Oceanographic convention).

set-up (Walker et al. 2004). We aim at presenting a new conceptual framework for the prediction of large waves based on the Tayfun (1980) and Janssen (2009) models coupled with Adler-Taylor (2009) theory on the Euler-characteristics of random fields. The framework so developed can be applied to study both second and third-order nonlinear effects and space-time properties of sea states where rogue waves are expected to occur. In particular, the new stochastic model describes the statistical structure of the wave surface using a Gram-Charlier type distribution for crest heights formulated in (Tayfun and Fedele 2007). This is able to capture the vertical crest-trough asymmetry induced by second-order nonlinearities measured by skewness (Tayfun 1980) as well as intermittency effects due to third-order nonlinearities measured by kurtosis (Janssen 2009). Moreover, the statistical properties of local waves in space and time are related to higher order moments of the wave directional spectrum capitalizing on Adler-Taylor (2009) theory. As a result, we are able to define the probability structure of the random variable η_{\max} representing the maximum third-order nonlinear surface wave height over an area in time. In accord with the new model, we will show that statistical averages of the maximum η_{\max} do not explain rare occurrences of large oceanic waves, which instead need to be interpreted using quantile-type approaches. In particular, we will consider the threshold h_q exceeded by η_{\max} with probability $0 \leq q \leq 1$ and the conditional mean $\bar{h}_q = \langle \eta_{\max} | \eta_{\max} > h_q \rangle$, where brackets denote statistical average. The statistic h_q is a generalization to space-time maxima of the threshold c_n exceeded by the crest height of the $1/n$ fraction of largest waves ob-

served at a point in time (Tayfun and Fedele 2007)). Similarly, \bar{h}_q generalizes the crest height average $c_{1/n}$ of the $1/n$ fraction of largest waves (Tayfun and Fedele 2007)).

The remainder of the paper is organized as follows. First, the essential elements of Janssen's (2003) formulation for the excess kurtosis of directional or short-crested seas are presented (Fedele 2015). This is followed by a review of the theory of Euler characteristics of random fields (Adler (1981)), space-time extremes (Fedele 2012) and associated stochastic wave groups (Fedele and Tayfun 2009). We then introduce a new stochastic model for the prediction of space-time extremes that accounts for both second and third-order nonlinearities. As a specific application here, capitalizing on the ERA-interim reanalysis (Dee et al. (2011)) and numerical simulations of the Andrea sea state (Bitner-Gregersen et al. 2014; Dias et al. 2015), the extreme statistics of the Andrea rogue-wave event is examined in detail. In concluding, we discuss the implications of these results on rogue-wave predictions.

2. Excess kurtosis of short-crested seas

Fedele (2015) revisited Janssen's (2003) formulation for the total excess kurtosis C_4 of weakly nonlinear gravity waves in deep water. This comprises a dynamic component C_4^d due to nonlinear wave-wave interactions (Janssen and Bidlot (2009)) and a bound contribution C_4^b (Janssen (2009)). For waves that are narrowband and characterized by a Gaussian type directional spectrum, C_4^d is expressed as a six-fold integral that depends on time t , BFI and the

parameter

$$R = \frac{\sigma_\theta^2}{2\nu^2}, \quad (3)$$

which is a dimensionless measure of short-crestedness of dominant waves, with ν and σ_θ denoting spectral bandwidth and angular spreading (Janssen and Bidlot (2009); Mori et al. (2011)). The associated excess kurtosis growth rate can be solved analytically for narrowband waves (Fedele (2015), see also Appendix A). It is found that in the focusing regime ($0 < R < 1$) the dynamic excess kurtosis initially grows attaining a maximum $C_{4,\max}$ at the intrinsic time scale

$$\tau_c = 2\pi\nu^2 \frac{t_c}{T_0} = \frac{1}{\sqrt{3R}}, \quad \text{or} \quad \frac{t_c}{T_0} \sim \frac{0.13}{\nu\sigma_\theta} \quad (4)$$

given by the least-squares fit

$$\frac{C_{4,\max}^d(R)}{BFI^2} \approx \frac{b}{(2\pi)^2} \frac{1-R}{R+bR_0}, \quad 0 \leq R \leq 1, \quad (5)$$

where $R_0 = \frac{3\sqrt{3}}{\pi}$ and $b = 2.48$. Eventually the excess dynamic kurtosis tends monotonically to zero as energy spreads directionally, as in the numerical simulations of Annenkov and Shrira (2009). In the defocusing regime ($R > 1$), the dynamic excess kurtosis is always negative. It attains a minimum at t_c given by (Janssen and Bidlot (2009))

$$C_{4,\min}^d \left(\frac{1}{R} \right) = -RC_{4,\max}^d(R), \quad 0 \leq R \leq 1. \quad (6)$$

and then tends to zero in the long time. Thus, the present theoretical predictions indicate a decaying trend for the dynamic excess kurtosis over large times.

For time scales $t \gtrsim 10t_c$, a cold start with initial homogeneous and Gaussian conditions become irrelevant as the wave field tends to a non-Gaussian state dominated by bound nonlinearities as the total kurtosis of surface elevations asymptotically approaches the value represented by the bound component (Annenkov and Shrira (2013, 2014)). In typical oceanic storms where dominant waves are characterized with $\nu \sim 0.2 - 0.4$ and $\sigma_\theta \sim 0.2 - 0.4$, this adjustment is rapid since the time scale $t_c/T_0 \sim O(1)$ with $T_0 \sim 10 - 14$ s and the dynamic kurtosis peak is negligible compared to the bound counterpart. For time scales of the order of or less than t_c , the dynamic component can dominate and the wave field may experience rogue wave behavior induced by quasi-resonant interactions (Janssen (2003)). However, one can argue that the large excess kurtosis transient observed during the initial stage of evolution is a result of the unrealistic assumption that the initial wave field is homogeneous Gaussian whereas oceanic wave fields are usually statistically inhomogeneous both

in space and time. In the left panel of Fig. 3, the preceding approximation in Eq. (5) is compared against the theoretical $C_{4,\max}^d$ for narrowband waves (Fedele (2015), see also Appendix A). Evidently, the latter is slightly larger than the maximum excess kurtosis derived by Janssen and Bidlot (2009), who have also used the fit in Eq. (5) but with $b = 1$. Their maximum follows by first taking the limit of the excess kurtosis at large times and then solving the associated six-fold integral (Fedele (2015)). Clearly, the dynamic excess kurtosis should vanish at large times. Janssen (personal communication, 2014) confirmed that Eq. (A3) holds and provided an alternative proof that the large-time C_4^d tends to zero using complex analysis.

Further, in the focusing regime ($R < 1$, $\tau_c < 1/\sqrt{3}$), from Eq. (5)

$$\frac{C_{4,\max}^d(\tau_c)}{BFI^2} \approx \frac{b}{(2\pi)^2} \frac{-1 + 3\tau_c^2}{1 + 3bR_0\tau_c^2}. \quad (7)$$

Clearly, the maximum kurtosis becomes larger for longer time scales τ_c , as illustrated in the right panel of Fig. 3. In the defocusing regime ($R > 1$, $\tau_c > 1/\sqrt{3}$), the dynamic excess kurtosis is negative and its minimum value $C_{4,\min}^d$ can be computed from Eq. (6). This result holds for deep-water waves. Drawing on Janssen and Onorato (2007) and Janssen and Bidlot (2009), the extension to intermediate waters of depth d follows by redefining the Benjamin-Feir Index as $BFI_S^2 = \alpha_S BFI^2$, where the depth factor α_S depends upon the dimensionless depth k_0d , where k_0 is the dominant wavenumber (see Appendix A). In this work we choose k_0 as the mean wavenumber k_m corresponding to the mean spectral frequency $\omega_m = m_{001}/m_{000}$, where m_{ijk} are spectral moments (see Appendix B). In the deep-water limit α_S becomes 1, and BFI_S reduces to the usual definition of BFI (Janssen (2003)). As the dimensionless depth k_0d decreases, BFI_S^2 reduces and it becomes negative for $k_0d < 1.363$ and so the dynamic excess kurtosis.

Thus, we expect that third-order quasi-resonant interactions do not play any role in the formation of large waves in realistic oceanic seas. However, the effects of bound nonlinearities on skewness and kurtosis should be accounted for in the extreme value analysis. In this regard, Janssen (2009) deeply investigated the properties of weakly nonlinear water waves within the Hamiltonian formalism developed by Krasitskii (1994). Further, he derived general expressions for skewness and kurtosis of the wave surface valid for finite depths and arbitrary spectra. In particular, the canonical transformation for a third-order narrowband (NB) wavetrain can be evaluated explicitly and Janssen (2009) gives a simple expression for the NB bound kurtosis given in Eq. (A4) of Appendix A.

Bitner-Gregersen et al. (2014) and Dias et al. (2015) performed Monte Carlo simulations of the hindcasted sea state in which the Andrea wave occurred using the irrotational and inviscid Euler equations. The estimated kurtosis

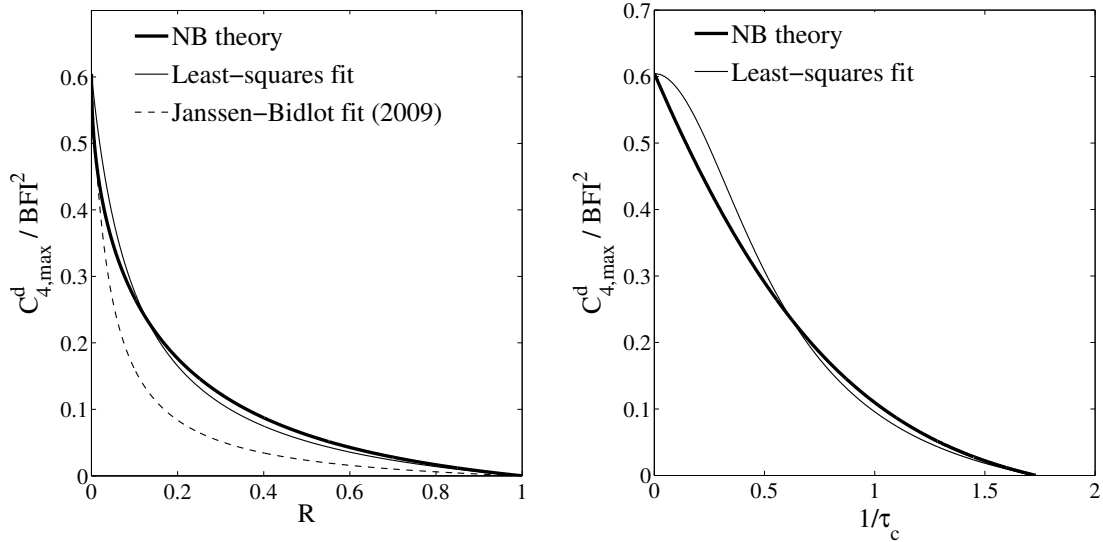


FIG. 3. Maximum dynamic excess kurtosis $C_{4,\max}^d$ as a function of (left) R and (right) $1/\tau_c$: (bold curve) present theoretical prediction, (thin curve) least-squares fit from Eq. (5) ($b = 2.48$) and (dashed curve) Janssen-Bidlot (2009) fit ($b = 1$).

is mainly due to non-resonant wave-wave interactions and $C_4 = C_4^b \sim 0.033$, or $\lambda_{40} = \lambda_{40}^b = 3C_4 \sim 0.1$. This is in fair agreement with Janssen's NB estimate $\lambda_{40}^{b,NB} = 0.09$ from Eq. (A4) using ERA-interim data. Bitner-Gregersen et al. (2014) also reported a larger kurtosis (~ 0.35) several hours before the Andrea wave occurrence. The actual laser measurements at Ekofisk give instead oscillating values within the range $0 - 0.3$ indicating unstable estimates of kurtosis as they are based on short 20-min time series ((Magnusson and Donelan 2013)).

Drawing on the ERA-interim reanalysis data, we now consider the hindcasted sea state during which the Andrea wave occurred (UTC 00 on Nov 9th, 2007). The top panel on the left of Fig. 4 shows the spatial distribution of significant wave height. The maximum H_s is about 8.3 m, which is smaller than 9.2 m actually observed (Magnusson and Donelan (2013)). It is well known that ERA-interim underestimates peak values and predicts broader directional spectra because of the low space and time resolution of the data. Indeed, wave parameters are solved every 6 hours and the grid cell areal size is $A_0 \sim 100^2$ km² with 60 vertical levels (Dee et al. (2011)). Nevertheless, such predictions provide leading order estimates of the sea-state parameters that can be refined further in future studies, using forecast models with higher resolution (Ponce de León and Guedes Soares (2014)). The top panels of Fig. 5 shows the Gaussian adjustment time t_c/T_0 and the Janssen NB total excess kurtosis $\lambda_{40} = 3C_4$. The NB dynamic component $\lambda_{40}^d = 3C_4^d$ from Eq. (5) and the bound counterpart $\lambda_{40}^b = 3C_4^b$ from Eq. (A4) are shown in the bottom panels of the same figure. At the Ekofisk location the water depth is $d = 74$ m, so $k_0 d \sim 3$ and $\alpha_S = 0.58$. As a

result the dynamic kurtosis is roughly half the corresponding value in deep waters, which is already negligible as the sea state is broadband. Clearly, the Gaussian adjustment time $t_c \sim O(T_0) \sim 15$ seconds, indicating that non-linear wave-wave interactions are negligible. Indeed, C_4^d is slightly negative, implying a defocusing wave regime due to the short-crestedness of the sea state whereas the non-zero and positive C_4^b component indicates that bound nonlinearities are not negligible.

Clearly, to date numerical simulations of the Euler equations are computationally expensive and unfeasible for an operational forecasting of extreme waves. One should consider Janssen's general third-order expression for kurtosis, which is valid for any depth and arbitrary spectra. This is a complex formula whose implementation requires care and effort beyond the scope of this paper.

In this work we propose that statistical predictions of extreme waves of realistic oceanic seas can be based on Adler-Taylor's (2009) theory of random fields coupled with the Tayfun (1980) and Janssen (2009) models to account for both second and third-order nonlinearities. In the following, we will first present the theory of space-time extremes for Gaussian seas (Fedele (2012)). Adler-Taylor theory is then extended to third-order non-Gaussian seas and apply it to study the statistical properties of the Andrea rogue wave event.

3. Space-time (ST) extremes

In accord with ERA-interim reanalysis, we can assume that sea states are both stationary in a time interval $D \leq D_{\text{ERA}} = 6$ hours and homogeneous over an area

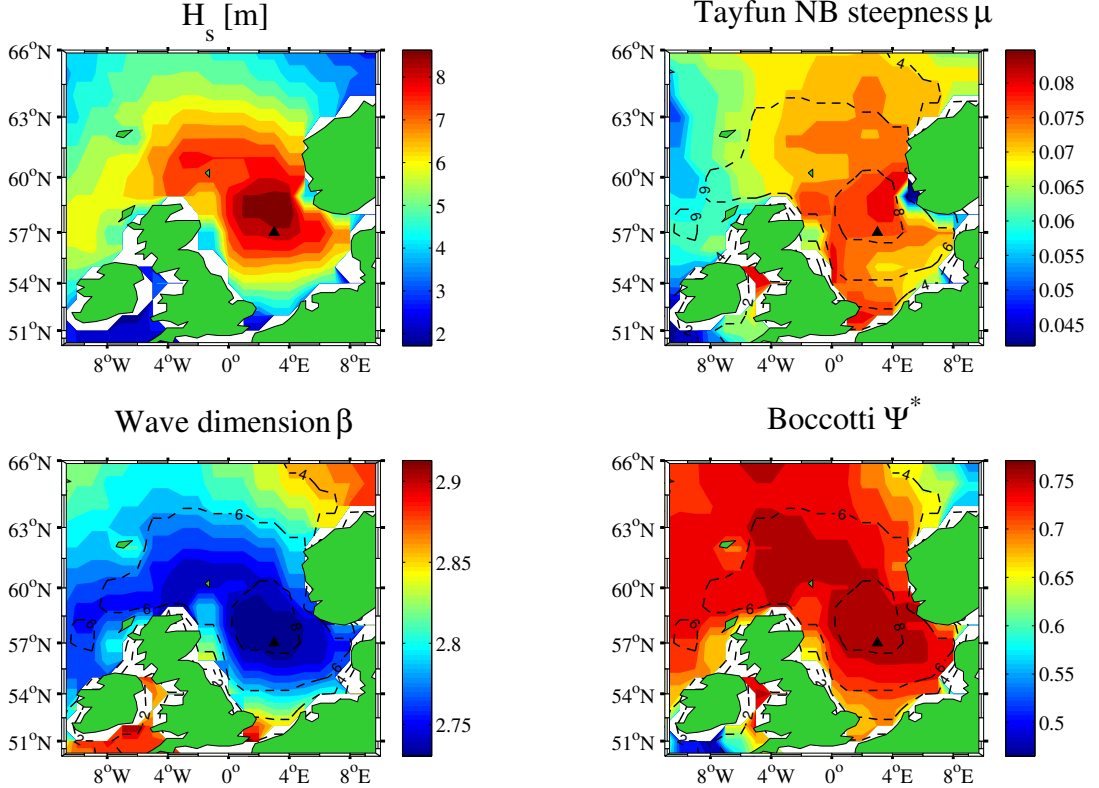


FIG. 4. ERA-interim reanalysis at the peak of the Andrea storm. Top panels: (left) significant wave height $H_s = 4\sigma$ and (right) Tayfun NB wave steepness μ_S (Eq. (22)). Bottom panels: (left) wave dimension β (Eq. (12)) and (right) narrowbandedness Boccotti parameter Ψ^* . Dashed lines are H_s contours. The triangle symbol indicates the Ekofisk site position.

$A \leq A_{ERA} = 100^2 \text{ km}^2$. Then, the free surface $\eta(\mathbf{x}, t)$ can be modeled as a three-dimensional (3-D) homogeneous Gaussian random field over the space-time volume Ω defined by the area A and the time interval D , and $\mathbf{x} = (x, y)$ denotes the horizontal coordinate vector. Thus, the associated probability distributions at any point of the volume is the same and Gaussian. Drawing on Adler (1981), we next consider the Euler characteristics (EC) of excursion sets of η defined as follows. Given a threshold z , the excursion set $U_\Omega(z)$ is the part of Ω within which η is above z :

$$U_\Omega(z) = \{(\mathbf{x}, t) \in \Omega : \eta(\mathbf{x}, t) > z\}. \quad (8)$$

In 1-D Gaussian processes, the EC simply counts the number of z -upcrossings. Thus, (8) provides the generalization of this concept to higher dimensions. Indeed, for two dimensional (2-D) random fields, EC counts the number of connected components minus the number of holes of the respective excursion set. In 3-D sets instead, EC counts the number of connected volumetric components of the set, minus the number of holes that pass through

it, plus the number of hollows inside. Further, the probability of exceedance that the global maximum of η over Ω , say η_{\max} , exceeds z depends on the domain size and it is well approximated by the expected EC of the excursion set, provided that z is sufficiently high (Adler (1981, 2000); Adler and Taylor (2009)). Intuitively, as z increases the holes and hollows in the excursion set $U_\Omega(z)$ disappear until each of its connected components includes just one local maximum of η , and EC counts the number of local maxima. For very large thresholds, EC equals 1 if the global maximum exceeds the threshold and 0 otherwise. Thus, EC of large excursion sets is a binary random variable with states 0 and 1, and, for large z ,

$$\Pr\{\eta_{\max} > z\} = \Pr\{EC(U_\Omega(z)) = 1\} = \langle EC(U_\Omega(z)) \rangle, \quad (9)$$

where angled brackets denote expectation. This heuristic identity has been proved rigorously to hold up to an error that is in general exponentially smaller than the expected EC approximation (Adler and Taylor (2009); Adler (2000)). For 3-D random fields, which are of interest in oceanic applications, the probability $P_{ST}(\xi; A, D)$ that the

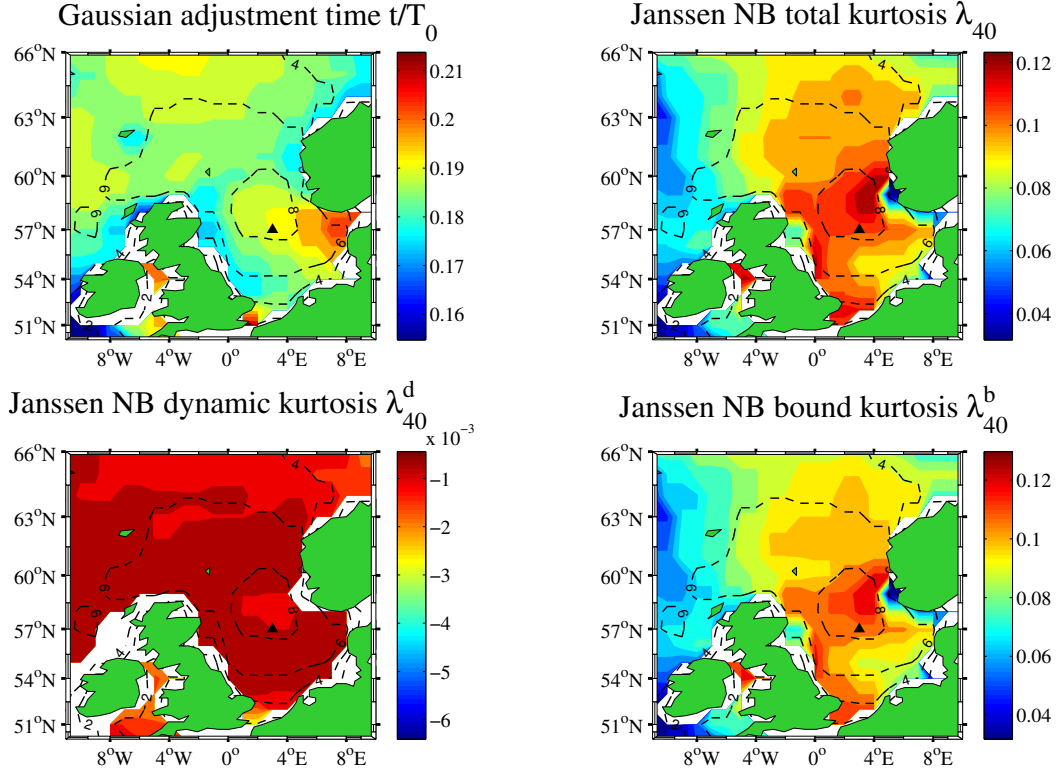


FIG. 5. ERA-interim reanalysis at the peak of the Andrea storm. Top panels: (left) Gaussian adjustment time t_c/T_0 (Eq. (4)) and (right) total NB kurtosis $\lambda_{40} = \lambda_{40}^d + \lambda_{40}^b$. Bottom panels: (left) NB dynamic kurtosis λ_{40}^d (Eq. (5)) and (right) NB bound kurtosis λ_{40}^b . Dashed lines are H_s contours [m]. The triangle symbol indicates the Ekofisk site position.

maximum surface elevation η_{\max} over the area A and during a time interval D exceeds the threshold ξH_s is given by (Adler and Taylor (2009))

$$P_{\text{ST}}(\xi; A, D) = \Pr\{\eta_{\max} > \xi H_s\} = (16M_3\xi^2 + 4M_2\xi + M_1)P_{\text{R}}(\xi), \quad (10)$$

where

$$P_{\text{R}}(\xi) = \Pr\{h > \xi H_s\} = \exp(-8\xi^2) \quad (11)$$

is the Rayleigh exceedance probability of the crest height h of a time wave observed at a single point within A . Here, M_1 and M_2 are the average number of 1-D and 2-D waves that can occur on the edges and boundaries of the volume Ω , and M_3 is the average number of 3-D waves that can occur within the volume (Fedele (2012)). These all depend on the directional wave spectrum and are given in Appendix A.

A statistical indicator of the geometry of space-time extremes in the volume Ω is the wave dimension β defined by Fedele (2012) as

$$\beta = 3 - \frac{4M_2\xi_m + 2M_1}{16M_3\xi_m^2 + 4M_2\xi_m + M_1}, \quad (12)$$

where ξ_m is the most probable surface elevation, or modal value which, according to Gumbel (1958) and Eq. (10), satisfies

$$P_{\text{ST}}(\xi_m; A, D) = (16M_3\xi_m^2 + 4M_2\xi_m + M_1)P_{\text{R}}(\xi_m) = 1. \quad (13)$$

Drawing on Fedele (2012), the correct average number of space-time waves of dimension β occurring within the space-time volume Ω spanned by area A and time interval D is

$$N_{\text{ST}}(A, D) = \frac{16M_3\xi_m^2 + 4M_2\xi_m + M_1}{(4\xi_m)^\beta}. \quad (14)$$

The parameter β represents a scale dimension of waves, i.e. the relative scale of a space-time wave with respect to the volume's size and $1 \leq \beta \leq 3$. In particular, if wave extremes are 3-D ($\beta > 2$) they are expected to occur within the volume Ω away from the boundaries, whereas the limiting case of 1-D time extremes ($\beta \sim 1$) occur for time waves observed at a single point. Furthermore, Fedele (2012) showed that space-time extremes are larger than

time extremes in agreement with recent stereo measurements of oceanic sea states (Fedele et al. (2013), see also Fig. 7).

The bottom-left panel of Fig. 4 shows the map of the estimated wave dimension β for the North Sea area at the peak time of the Andrea storm for sea states of duration $D = 3$ hours over the cell area A_{ERA} . Clearly, sea states were short-crested and extremes are roughly 3-D, indicating that the area considered is large compared to the mean wavelength. Thus, in accord with Boccotti's (2000) QD theory, a space-time extreme most likely coincides with the crest of a focusing wave group that passes through the area as described below.

4. Extreme nonlinear wave groups

Drawing on Boccotti's (2000) QD theory, Fedele and Tayfun (2009) showed that for second-order weakly nonlinear waves the expected space-time dynamics near a large wave crest is that of a stochastic wave group whose free surface is described by

$$\zeta_c/H_s = \xi_0\zeta_1 + \xi_0^2\zeta_2, \quad (15)$$

where $\xi_0 = h_0/H_s$ is the dimensionless linear crest height,

$$\zeta_1(\mathbf{X}, T) = \Psi(\mathbf{X}, T) \quad (16)$$

is the linear component,

$$\begin{aligned} \Psi(\mathbf{X}, T) &= \frac{\langle \eta(\mathbf{x}, t)\eta(\mathbf{x} + \mathbf{X}, t + T) \rangle}{\sigma^2} \\ &= \int \frac{S_1}{\sigma^2} \cos(\chi_1) d\omega_1 d\theta_1 \end{aligned} \quad (17)$$

is the space-time covariance of η (Boccotti (2000)) and

$$\begin{aligned} \zeta_2 &= \int \frac{S_1 S_2}{\sigma^3} \left(A_{12}^+ \cos(\chi_1 + \chi_2) + \right. \\ &\quad \left. A_{12}^- \cos(\chi_1 - \chi_2) \right) d\omega_1 d\theta_1 d\omega_2 d\theta_2 \end{aligned} \quad (18)$$

is the second-order correction. Here, $S_j = S(\omega_j, \theta_j)$ and $\chi_j = \mathbf{k}_j \cdot \mathbf{X} - \omega_j T$, where $\mathbf{X} = (X, Y)$ and $\mathbf{k}_j = (k_j \sin \theta_j, k_j \cos \theta_j)$ with $k_j \tanh(k_j d) = \omega_j^2/g$ from linear dispersion, and the coefficients A_{12}^\pm can be found in Sharma and Dean (1979). For generic sea states, the largest nonlinear crest amplitude is attained at the focusing point ($\mathbf{X} = \mathbf{0}, T = 0$) and given by

$$\xi = \xi_0 + 2\mu\xi_0^2, \quad (19)$$

where $\xi = h/H_s$ is the nonlinear crest height. The Tayfun wave steepness $\mu = C_3/3$ relates to the wave skewness C_3 of surface elevations. For oceanic applications in deep waters, Fedele and Tayfun (2009) proposed the approximation

$$\mu \sim \mu_a = \mu_m (1 - \nu + \nu^2), \quad (20)$$

where $\mu_m = k_m \sigma$, which is an upper bound for C_3 . From the linear dispersion relation $k_m = \omega_m^2/g$ is the wavenumber corresponding to the mean spectral frequency $\omega_m = m_{001}/m_{000}$,

$$\nu = \sqrt{m_{000}m_{002}/m_{001}^2 - 1} \quad (21)$$

is the spectral bandwidth and m_{ijk} are spectral moments (see Appendix B). In intermediate water depths, the narrowband approximations lead to (Tayfun 2006)

$$\mu \sim \mu_s = \mu_m f_s, \quad (22)$$

where $f_s = D_1 + D_2$, with

$$\begin{aligned} D_1 &= \frac{1}{2} \frac{4n-1}{n^2 \tanh(q_m) - q_m}, \\ D_2 &= \frac{\cosh(q_m) [2 + \cosh(2q_m)]}{2 \sinh^3(q_m)}, \end{aligned}$$

$n = [1 + 2q_m/\sinh(2q_m)]/2$, $q_m = k_m d$ and d is the water depth. The coefficients D_1 and D_2 arise from the frequency-difference and frequency-sum terms, i.e. A_{12}^- and A_{12}^+ , in Eq. (18) as the spectral bandwidth $\nu \rightarrow 0$. A general expression for skewness valid for finite depths and arbitrary spectra is given by Janssen (2009). The NB limit of Janssen's skewness yields the same Eq. (22) derived by Tayfun (2006).

Further, the wave trough following the large crest occurs at $t = T^*$, where T^* is the abscissa of the first minimum of the time covariance $\psi(T) = \Psi(\mathbf{X} = \mathbf{0}, T)$ (Boccotti 2000). Second-order nonlinearities do not affect the crest-to-trough heights of large waves since wave crests and troughs are displaced upward equally. Thus, the maximum second-order nonlinear crest-to-trough height observed at a point in time remains essentially the same as that of the linear group ζ_1 and given by $H/H_s = \xi_0(1 + \psi^*)$, where $\psi^* = \psi(T^*)$ is the Boccotti's (2000) narrowbandedness parameter. Note that for narrowband waves $\psi^* \rightarrow 1$. The left panels of Fig. 4 show the maps of the Tayfun NB steepness μ (top) from Eq. (22) and Boccotti ψ^* (bottom) estimated from the hindcasted ERA-interim sea state in which the Andrea wave occurred. It appears that $\psi^* \sim 0.75$ as the characteristic value of short-crested sea states dominated by wind waves (Boccotti (2000)). At the Ekofisk location, the NB prediction gives $\mu = C_3/3 \sim 0.05$ in fair agreement with the predicted values from numerical simulations of the Euler equations (Bitner-Gregersen et al. 2014; Dias et al. 2015) and actual laser measurements (Magnusson and Donelan 2013)).

We have shown that that third-order quasi-resonant interactions do not play any role in the formation of large waves in realistic oceanic seas. However, the effects of third-order bound nonlinearities on the prediction of maximum crest and wave heights must be accounted for as addressed in the next section.

5. A new stochastic third-order space-time (FST) model

Drawing on Fedele (2008, 2012) and Tayfun and Fedele (2007), we propose a new stochastic model, hereafter referred to as *FST*, which accounts for both second and third-order nonlinearities in the prediction of space-time extremes. In particular, consider a 3-D non-Gaussian field over an area A for a time period of D . Clearly, the area cannot be too large since the wave field may not be homogeneous. The duration should be short so that spectral changes occurring in time are not so significant and the sea state can be assumed as stationary. Then, the third-order nonlinear probability $P_{\text{FST}}^{(nl)}(\xi; A, D)$ that the maximum surface elevation η_{max} over the area A and during the time interval D exceeds the generic threshold ξH_s is equal to the probability of exceeding the threshold ξ_0 , which accounts for kurtosis effects only, that is

$$P_{\text{FST}}^{(nl)}(\xi; A, D) = P_{\text{ST}}(\xi_0; A, D) (1 + \Lambda \xi_0^2 (4\xi_0^2 - 1)). \quad (23)$$

The Gaussian probability of exceedance P_{ST} is given in Eq. (10) and the amplitude ξ , which accounts for both skewness and kurtosis effects, relates to ξ_0 via the Tayfun (1980) quadratic equation

$$\xi = \xi_0 + 2\mu \xi_0^2. \quad (24)$$

Further, the parameter

$$\Lambda = \lambda_{40} + 2\lambda_{22} + \lambda_{04} \quad (25)$$

is a measure of third-order nonlinearities and it is a function of the fourth order cumulants λ_{nm} of the wave surface η and its Hilbert transform $\hat{\eta}$ (Tayfun and Fedele 2007)

$$\lambda_{nm} = \langle \eta^n \hat{\eta}^m \rangle / \sigma^{n+m} + (-1)^{m/2} (n-1)(m-1), \quad (26)$$

where σ is the standard deviation of the wave surface and $n+m=4$. Drawing on Mori and Janssen (2006), we assume the following relations between cumulants

$$\lambda_{22} = \lambda_{40}/3, \quad \lambda_{04} = \lambda_{40}, \quad (27)$$

and Eq. (25) simplifies to

$$\Lambda = \Lambda_{\text{appr}} = \frac{8\lambda_{40}}{3}, \quad (28)$$

which will be used in this work. Then, Eq. (23) reduces to a modified Edgeworth-Rayleigh (MER) distribution (Mori and Janssen 2006). For realistic oceanic seas the kurtosis $\lambda_{40} \sim \lambda_{40}^b$ is only due to bound nonlinearities. To date, the validity of the cumulant relations in Eq. (27) has been proven to hold for second-order NB waves only (Tayfun and Lo 1990). Further studies are desirable to determine the general expressions of fourth order cumulants of

the wave surface relying on Janssen's (2009) third-order Hamiltonian formulation, but this is beyond the scope of this paper.

Given the probability structure of the wave surface defined by Eq. (23), the nonlinear mean maximum surface or crest height $\bar{h}_{\text{FST}} = \xi_{\text{FST}} H_s$ attained over the area A during a time interval D is given, according to Gumbel (1958), by

$$\begin{aligned} \xi_{\text{FST}} &= \frac{\bar{h}_{\text{FST}}}{H_s} \\ &= \xi_m + 2\mu \xi_m^2 + \frac{\gamma_e (1 + 4\mu \xi_m)}{16\xi_m - \frac{32M_3\xi_m + 4M_2}{16M_3\xi_m^2 + 4M_2\xi_m + M_1} - \Lambda G(\xi_m)}, \end{aligned} \quad (29)$$

where the most probable surface elevation value ξ_m satisfies $P_{\text{FST}}(\xi_m; A, D) = 1$, or equivalently from Eq. (23)

$$(16M_3\xi_m^2 + 4M_2\xi_m + M_1)P_{\text{R}}(\xi_m) (1 + \Lambda \xi_m^2 (4\xi_m^2 - 1)) = 1,$$

and

$$G(\xi_m) = \frac{2\xi_m(8\xi_m^2 - 1)}{1 + \Lambda \xi_m^2 (4\xi_m^2 - 1)}.$$

The nonlinear mean maximum surface or crest height h_{T} expected at a point during the time interval D follows from Eq. (29) by setting $M_2 = M_3 = 0$ and $M_1 = N_{\text{D}}$, namely

$$\xi_{\text{T}} = h_{\text{T}}/H_s = \xi_m + 2\mu \xi_m^2 + \frac{\gamma_e (1 + 4\mu \xi_m)}{16\xi_m - \Lambda G(\xi_m)}, \quad (30)$$

where, now, ξ_m satisfies

$$N_{\text{D}}P_{\text{R}}(\xi_m) (1 + \Lambda \xi_m^2 (4\xi_m^2 - 1)) = 1.$$

Here, $N_{\text{D}} = D/\bar{T}$ denotes the number of wave occurring during D and \bar{T} is the mean up-crossing period (see Appendix B). The linear mean counterpart follows from Eq. (30) by setting $\mu = 0$ and $\Lambda = 0$.

Drawing on the Boccotti (2000) distribution for wave heights, the third-order nonlinear mean maximum wave height expected at a point is given by

$$\bar{H}_{\text{T}} = \bar{h}_{\text{T}}^{(\Lambda)} \sqrt{2(1 + \psi^*)}, \quad (31)$$

where $\bar{h}_{\text{T}}^{(\Lambda)}$ is the nonlinear mean maximum crest height that accounts for kurtosis effects only. This follows from Eq. (30) by setting $\mu = 0$, namely

$$\bar{h}_{\text{T}}^{(\Lambda)}/H_s = \xi_m + \frac{\gamma_e}{16\xi_m - \Lambda G(\xi_m)}, \quad (32)$$

where

$$N_{\text{D}}P_{\text{R}}(\xi_m) (1 + \Lambda \xi_m^2 (4\xi_m^2 - 1)) = 1.$$

For narrowband waves, $\psi^* = 1$ and Eq. (31) reduces to the MER model proposed by Mori and Janssen (2006).

Clearly, this overestimates wave heights in short-crested or multidirectional seas as, in general, $\psi^* < 1$.

When the lateral dimension $\ell = \sqrt{A}$ is much larger than the average wavelength L_0 , the maximum surface height occurs most likely within the area of interest and not on its boundaries. In this case, on average the number of 3-D waves is much larger than the numbers of 1-D and 2-D waves that can occur on the boundaries, i.e. $M_3 \gg M_2$ and M_1 . Keeping only the leading term in Eq. (29) yields the following asymptotic value of the expected surface wave height maximum over large areas

$$\xi_{\text{FST}}^{(3D)} = \frac{h_{\text{FST}}^{(3D)}}{H_s} = \xi_m + 2\mu\xi_m^2 + \frac{\gamma_e(1 + 4\mu\xi_m)}{16\xi_m - \frac{2}{\xi_m} - \Lambda G(\xi_m)}, \quad (33)$$

where

$$16M_3\xi_m^2 P_R(\xi_m) (1 + \Lambda\xi_m^2(4\xi_m^2 - 1)) = 1.$$

For 2-D waves only ($M_1 = M_3 = 0$ in Eq. (29))

$$\xi_{\text{FST}}^{(2D)} = \frac{\xi_{\text{FST}}^{(2D)}}{H_s} = \xi_m + 2\mu\xi_m^2 + \frac{\gamma_e(1 + 4\mu\xi_m)}{16\xi_m - \frac{1}{\xi_m} - \Lambda G(\xi_m)}, \quad (34)$$

where

$$4M_2\xi_m P_R(\xi_m) (1 + \Lambda\xi_m^2(4\xi_m^2 - 1)) = 1.$$

If one ignores kurtosis effects ($\Lambda = 0$), Eqs. (33) and (34) reduce to the 2-D and 3-D analogues of the Piterbarg-Tayfun (PT) model formulated by Socquet-Juglard et al. (2005), and hereafter referred to as 2D-PT and 3D-PT respectively (see also Piterbarg (1995) and Forristall (2011)).

In offshore applications, the interest is in the expected wave maxima over small areas such as those covered by oil rigs, i.e. $\ell \leq L_0$. In this range, Fedele et al. (2013) have shown that the boundary corrections accounted by both terms M_1 and M_2 are important for a correct estimation of Euler characteristics and expected maxima (see also Forristall (2015)). Hence, they cannot be ignored as has been assumed by Romolo and Arena (2015), since maximum surface heights expected over small areas are underestimated. This point is elaborated further in the next section and demonstrated explicitly by way of the results displayed in Fig. 7.

As an application, consider now the hindcasted sea state during which the Andrea wave occurred (wave steepness $\mu = C_3/3 \sim 0.05$ and excess kurtosis $\lambda_{40} = 3C_4 \sim 0.1$ from Dias et al. (2015)). The top panel of Fig. 6 displays the predictions from Eq. (30) for the third-order mean maximum surface or crest height \bar{h}_T expected at a point as a function of the excess kurtosis λ_{40} for a typical $D = 3$ -hour sea state. From Eq. 32, the mean height $\bar{h}_T^{(\Lambda)}$ that accounts for kurtosis effects only is also shown. Comparing

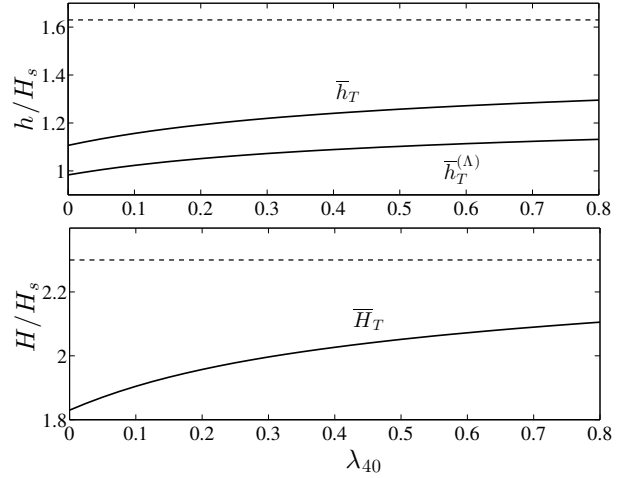


FIG. 6. Andrea wave: (top panel) nonlinear mean maximum surface or crest height \bar{h}_T expected at a point as a function of excess kurtosis λ_{40} , which accounts for both second-order (skewness) and third-order (kurtosis) nonlinearities. The prediction $\bar{h}_T^{(\Lambda)}$ of average heights that accounts for third-order kurtosis effects only is also shown. (Bottom panel) nonlinear mean maximum wave height expected at a point (\bar{H}_T) as a function of excess kurtosis λ_{40} . Dashed lines denote the actual Andrea crest and wave height values ($h_{\text{obs}} = 1.63H_s$ and $H_{\text{obs}} = 2.3H_s$).

the two predictions, it is clear that second-order nonlinearities cannot be neglected as they yield a substantial 15% increase in crest height in comparison to the modest 5% increase due to kurtosis (~ 0.1) from the linear estimates ($\lambda_{40} = 0$). Note that even for unrealistic values of kurtosis (~ 0.8) the predictions are well below the observed actual Andrea crest height $h_{\text{obs}} = 1.63H_s$ (dashed line). Further, the bottom panel of Fig. 6 displays the mean maximum wave height \bar{H}_T expected at a point from Eq. (31). This is smaller than the observed actual Andrea wave height $H_{\text{obs}} = 2.3H_s$.

In summary, averages of maxima do not explain the actual large Andrea time crest and wave heights observed at the measurement site. This point will be discussed and addressed later in section 7.

6. ST analysis of the Andrea wave

In this section we will study the space-time properties of the Andrea storm in comparison to stereo wave measurements at the Acqua Alta site of a short-crested sea state dominated by bora winds (experiment 2, see Fedele et al. (2013)). For example, Fig. 7 shows the prediction of space-time extremes at the Acqua Alta site and from the hindcasted ERA-interm Andrea sea state during which the rogue wave occurred. In particular, the left panel of the figure shows the Acqua Alta observed ratio of space-time and time maximum surface heights over a period of $D \sim 0.5$ hours as a function of the lateral dimension ℓ normalized to

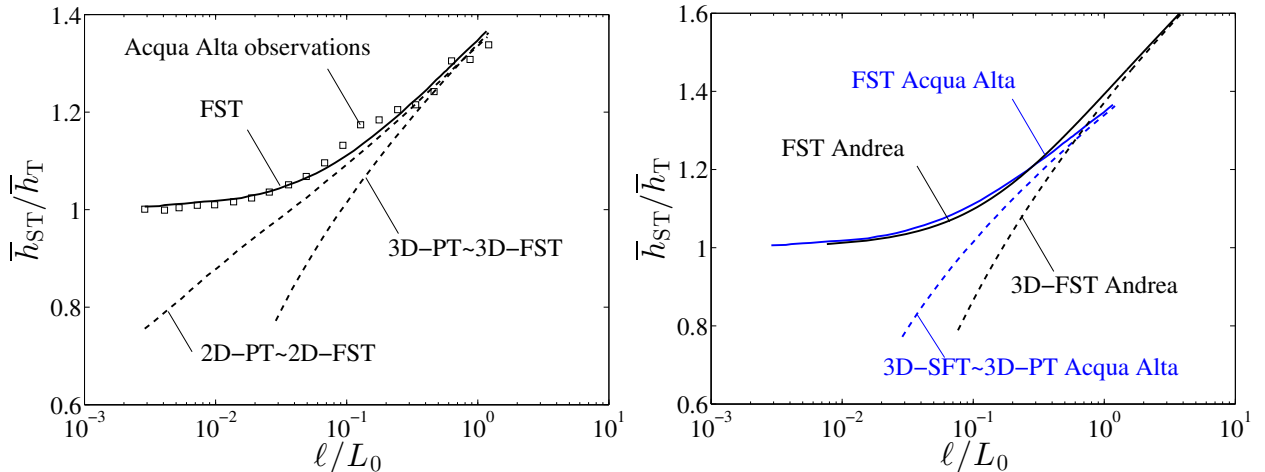


FIG. 7. Left panel, Acqua Alta stereo measurements (Fedele et al. (2013)): comparison between the observed ratio of space-time and time maximum surface heights (hollow squares) and theoretical averages \bar{h}_{FST}/\bar{h}_T as a function of the lateral side length ℓ normalized to the average wavelength L_0 . Fedele space-time (FST) model (solid line) and 2D and 3D Piterbag-Tayfun (PT) models nearly the same as 2D- and 3D-FST (dashed lines). Right panel, Andrea ERA-interim predictions: expected ratio of mean areal and point maximum surface heights estimated at the Ekofisk location (FST, black line; 3D-FST, dashed line). For comparison the estimated ratios for Acqua Alta are also shown (FST, blue solid line; 3D-FST 2D-PT, blue dashed line).

the average wavelength $L_0 \sim 19$ m (hollow squares, maximum length $\ell_{max} \sim 24$ m). In the same panel, we compare the theoretical FST ratio \bar{h}_{FST}/\bar{h}_T , which accounts for boundary corrections associated with M_1 and M_2 in Eq. (29), and the asymptotic 3D-FST from Eq. (33), which is valid over large areas and ignores boundary effects. The 2D-FST model from Eq. (34) is also shown. They both nearly coincide with 2D-PT and 3D-PT as the measured kurtosis at Acqua Alta was almost Gaussian. As one can see, the boundary contributions cannot be neglected over areas with lateral dimension comparable to or smaller than the typical wavelength. Indeed, both 2D- and 3D-FST underestimate the observed ratios when $\ell \leq L_0$. Note that for $\ell \sim L_0$ the observed space-time wave surface maximum \bar{h}_{FST} is 1.4 times larger than the time maximum \bar{h}_T at a single point.

A similar trend is also observed for the expected space-time extremes of the Andrea sea state for the same time period of $D = 0.5$ hours. Specifically, the right panel of Fig. 7 displays the mean maximum surface height ratios \bar{h}_{FST}/\bar{h}_T (FST, black curve) as a function of ℓ/L_0 estimated at the Ekofisk location, where the ERA-interim predicts a mean wavelength $L_0 \sim 150$ m. Note that the FST ratios for Acqua Alta and Andrea (blue and black solid curves) are close to each other for $\ell \leq L_0$. These results are very encouraging as the observed sea state at Acqua Alta was in deep waters (measured $H_s = 1.09$ m and $d/L_0 = 1.25$, with $d = 16$ m) whereas the Andrea sea state was in intermediate waters (ERA-interim estimates $H_s = 8.3$ m and $d/L_0 = 0.49$, with $d = 74$ m). Although ERA-interim un-

derestimates the actual value of H_s at Ekofisk ($= 9.2$ m), it appears that the maximum surface height ratio \bar{h}_{FST}/\bar{h}_T is slightly sensitive to the significant wave height level and just depends on average spectral properties of the sea state. Further studies are desirable to investigate possible statistical similarities and universal laws for space-time extremes in wind sea states, but this is beyond the scope of this paper.

Clearly, space-time extremes cannot explain the actual large Andrea time crest height observed at the measurement point. The space-time analysis of the Andrea storm simply predicts that the maximum surface wave height over the platform footprint area is $\sim 20\%$ higher than the average maximum surface height that is expected at a fixed point within the same area ($\ell/L_0 \sim 0.3$, see right panel of Fig. 7). Indeed, in relatively short-crested directional seas such as those observed around the Ekofisk area, it is very unlikely that the observed crest actually coincides with the largest crest of a group of waves propagating in space-time. In contrast, in accord with Boccotti's (2000) QD theory, it is most likely that the sea surface was in fact much higher somewhere near the measurement point.

7. Threshold h_q exceeded with probability q by the maximum surface height

Consider the average duration of $D = 3$ hours for the Andrea sea state in which the rogue wave was observed, considering that the ERA time resolution is of $D_{ERA} = 6$ hours. Monte Carlo simulations yield wave steepness $\mu \sim 0.05$ and excess kurtosis $\lambda_{40} \sim 0.1$ (Bitner-Gregersen et al.

2014; Dias et al. 2015). It follows that the mean maximum nonlinear wave surface height \bar{h}_T expected at a point is $\sim 1.2H_s$ (see Fig. (6)). This is lower than the actual value $h_{obs} \sim 1.63H_s$ observed. Statistically, this means that in an ensemble of M realizations of 3-hour sea states, each of which has similar statistical structure to the Andrea wave field, all the maximum surface heights observed at a point will exceed $1.2H_s$. Clearly, the maximum surface height at a point can reach or exceed the actual observed value $1.63H_s$ only in few realizations out of the ensemble of M sea states.

To characterize such rare occurrences in weakly nonlinear third-order random seas one can consider the threshold $h_q = \xi_q H_s$ exceeded with probability $0 \leq q \leq 1$ by the maximum surface height η_{max} over an area A during a sea state of duration D . This satisfies (see Appendix C)

$$P_{FST}^{(nl)}(\xi_q; A, D) = q, \quad (35)$$

where $\xi_q = \xi_{0,q} + 2\mu\xi_{0,q}^2$, $\xi_{0,q}$ follows from Eq. (C5) and the nonlinear probability of exceedance $P_{FST}^{(nl)}$ is given in Eq. (23). Further, the conditional mean $\bar{h}_q = \langle \eta_{max} | \eta_{max} > h_q \rangle$ is given by

$$\bar{h}_q = h_q + (\chi_{1,q} + \mu\chi_{2,q} + \Lambda\chi_{3,q} + \mu\Lambda\chi_{4,q})H_s/q, \quad (36)$$

where the coefficients $\chi_{j,q}$ depend on q as well as on the spectral parameters M_j and ξ_q . For Gaussian waves, the linear threshold $h_q^{(L)}$ and conditional mean $\bar{h}_q^{(L)}$ follow by setting both $\mu = 0$ and $\Lambda = 0$ in Eqs. (35) and (36) respectively. For second-order waves the associated threshold $h_q^{(\mu)}$ and mean $\bar{h}_q^{(\mu)}$ follow by setting $\Lambda = 0$ only. As q becomes smaller the threshold h_q tends to coincide with the mean \bar{h}_q since terms $\chi_{j,q}/q$ in Eq. (36) tend to zero, and similarly for linear and second-order thresholds.

In this work, we consider the time thresholds $h_{T,q}^{(L)}$, $h_{T,q}^{(\mu)}$ and $h_{T,q}$ at a point and conditional averages $\bar{h}_{T,q}^{(L)}$, $\bar{h}_{T,q}^{(\mu)}$ and $\bar{h}_{T,q}$. These can be computed using $M_2 = M_3 = 0$ and $M_1 = N_D$ in Eqs. (35) and (36). Here, N_D denotes the number of zero-crossing waves occurring during the time interval D . Further, note that $\bar{h}_{T,q=1}$ coincides with the mean maximum third-order surface height \bar{h}_T and similarly for linear and second-order conditional averages, that is $\bar{h}_{T,1}^L = \bar{h}_T^L$ and $\bar{h}_{T,1}^{(\mu)} = \bar{h}_T^{(\mu)}$.

Drawing on the Boccotti (2000) distribution for wave heights, the third-order nonlinear threshold exceeded with probability q by the maximum wave height at a point is given by

$$H_{T,q} = h_{T,q}^{(\Lambda)} \sqrt{2(1 + \psi^*)}, \quad (37)$$

and the conditional mean

$$\bar{H}_{T,q} = \bar{h}_{T,q}^{(\Lambda)} \sqrt{2(1 + \psi^*)}. \quad (38)$$

Here, the threshold $h_{T,q}^{(\Lambda)}$ accounts for kurtosis effects only and it follows from Eq. (35) with $\mu = 0$. Similarly, the conditional mean $\bar{h}_{T,q}^{(\Lambda)}$ follows from Eq. (36). For Gaussian waves, the linear counterparts are given by

$$H_{T,q}^{(L)} = h_{T,q}^{(L)} \sqrt{2(1 + \psi^*)} \quad (39)$$

and

$$\bar{H}_{T,q}^{(L)} = \bar{h}_{T,q}^{(L)} \sqrt{2(1 + \psi^*)}. \quad (40)$$

Note that $\bar{H}_{T,q=1}$ coincides with the mean maximum nonlinear wave height \bar{H}_T and the linear conditional mean $\bar{H}_{T,1}^L = \bar{H}_T^L$.

The statistical interpretation of the threshold h_q and conditional mean \bar{h}_q is as follows. Consider M realizations of a stationary and homogeneous sea state of duration D . On this basis, there would be M samples, say $(\eta_{max}^{(1)}, \dots, \eta_{max}^{(M)})$ of the maximum surface height η_{max} observed within an area A during the time interval D . Then, the threshold h_q is exceeded in only qM realizations of the ensemble of M sea states, and \bar{h}_q is the average of the qM largest values in the sample. Similar interpretation holds for the threshold H_q and conditional mean \bar{H}_q for the maximum wave height.

For the time statistics at a point, $h_{T,q}$ coincides with the standard threshold c_n exceeded by the crest heights of the $1/n$ fraction of largest waves if we set $n = N_D/q$, where N_D is the average number of zero-crossing waves expected in a D -hour sea state. Similarly, $\bar{h}_{T,q}$ is the crest height average $c_{1/n}$ of the q/N_D fraction of largest time waves (see, for example, Tayfun and Fedele (2007)). Clearly, the previous interpretation does not hold for space-time or multidimensional random fields. Indeed, the notion of zero-upcrossings is generalized to that of Euler Characteristics of excursion sets and wave counting is not as obvious as in one-dimensional random processes as there is no clear definition of a space-time wave (Fedele 2012).

Consider now the hindcasted ERA-interim Andrea sea state during which the rogue wave occurred. Fig. 8 displays the third-order threshold $h_{T,q}$ from Eq. (36) for the maximum crest height at a point as a function of the exceedance probability q for a 3-hour sea state (thin black line). The linear $h_{T,q}^{(L)}$ (thin red line) and second-order threshold $h_{T,q}^{(\mu)}$ (thin blue line) are also shown in the same figure. The corresponding conditional averages are also displayed (bold lines). If we account for both second and third-order nonlinearities, the actual crest height point measurement observed ($h_{obs} \sim 1.63H_s$) nearly coincides with $h_{T,1/1000} \sim 1.62H_s$. Thus, only in 1 sea state out of the ensemble the maximum surface height exceeds $1.62H_s$.

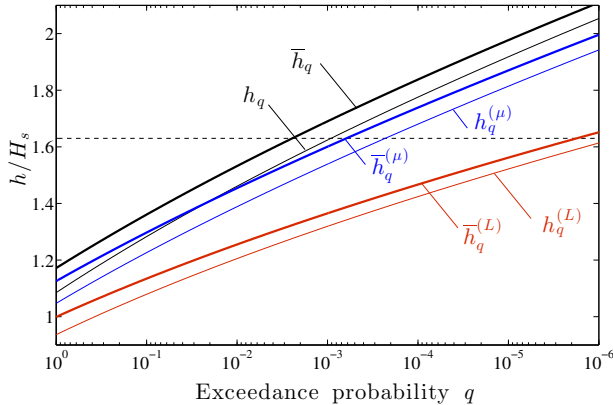


FIG. 8. Andrea wave: third-order nonlinear threshold $h_{T,q}$ for the maximum crest height at a point as a function of the exceedance probability q for a 3-hour sea state (thin black line). The linear threshold $h_{T,q}^{(L)}$ (thin red line) and the second-order threshold $h_{T,q}^{(\mu)}$ (thin blue line) are also shown. The conditional averages \bar{h}_q , $h_{T,q}^{(\mu)}$ and $\bar{h}_q^{(L)}$ are also displayed (bold lines). The horizontal dashed line indicates the actual Andrea wave crest value. Note that $\bar{h}_{T,q=1}$ coincides with the mean maximum surface height \bar{h}_T and similarly for linear and second-order conditional averages, i.e. $\bar{h}_{T,1}^L = \bar{h}_T^L$ and $\bar{h}_{T,1}^{(\mu)} = \bar{h}_T^{(\mu)}$. The wave steepness $\mu \sim 0.05$ and the excess kurtosis $\lambda_{40} \sim 0.1$ (Bitner-Gregersen et al. 2014; Dias et al. 2015).

For second-order nonlinearities only, h_{obs} is slightly below $h_{T,1/10,000}^{(\mu)} \sim 1.68H_s$ (thin blue line). Further, h_{obs} exceeds the linear $h_{T,1/100,000}^{(L)} \sim 1.52H_s$ and it nearly coincides with $h_{T,1/1,000,000}^{(L)}$ making the Andrea wave event an extremely rare occurrence in Gaussian seas.

The predictions for the maximum wave height at a point are shown in Fig. (9). Note that the actual wave height observed at Andrea ($H_{obs} \sim 2.3H_s$) exceeds the third-order threshold $H_{T,1/10} = 2.13H_s$ and it nearly coincides with the linear $H_{T,1/100}^{(L)} = 2.26H_s$. This indicates that the Andrea wave most likely occurred in the configuration of a maximum crest and the associated wave height was not the largest and not as extreme as the crest height. Indeed, according to Boccotti's (2000) QD theory, extreme waves with the largest wave height have almost symmetrical crests and troughs, but the Andrea wave had a strong crest-trough asymmetry (Magnusson and Donelan (2013)).

Note that $h_{T,1/1,000}$ is the same as the threshold $c_{1,000,000}$ exceeded by the crest of one wave in a sample of $n = N_D/q = 10^6$ waves, where $q = 10^{-3}$ and $N_D \sim 10^3$ (mean period ~ 12 s). Thus, in ideal stationary conditions that last forever the Andrea crest height h_{obs} is exceeded in average every $R = 0.5$ years. However, oceanic seas are non-stationarity and a long-term analysis of storms is required to estimate the probability of occurrence P_s of a D -hour sea state as that similar to the Andrea field. Then,

the probability that the threshold h_q is exceeded during the lifetime span L of an offshore structure is $P = P_s q$, which is an important design parameter. The associated return period R follows from the relation $P = \exp(-L/R)$, which assumes a Poisson statistics for storm occurrences (Boccotti 2000). Such an analysis requires predicting extremes of non-stationary wave fields following Haver (2002) (see also (Boccotti 2000; Fedele 2012)), but this is beyond the scope of this paper.

In summary, second-order skewness nonlinearities of crest heights are dominant as also indicated by extensive statistical analyses of oceanic wave measurements (Tayfun and Fedele 2007; Tayfun 2008; Fedele 2008; Fedele and Tayfun 2009). Further, in accord with Janssen (2003), bound kurtosis effects cannot be neglected and must be accounted for in order to obtain more accurate estimates of both crest and wave height extremes.

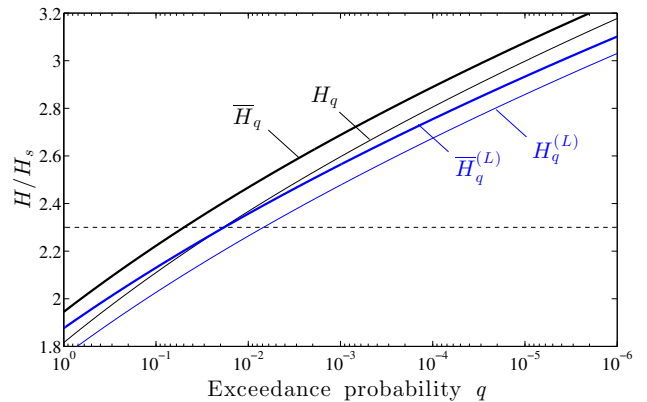


FIG. 9. Andrea wave: (top) linear and nonlinear thresholds $H_q^{(L)}$ and H_q (thin lines) of the maximum wave height at a point as a function of the exceedance probability q for a 3-hour sea state. The conditional averages $\bar{H}_q^{(L)}$ and \bar{H}_q (bold lines) are also shown. The horizontal dashed line indicates the actual Andrea wave height value. Note that $\bar{H}_{T,q=1}^{(L)}$ coincides with the mean maximum wave height \bar{H}_T and similarly the linear conditional average $\bar{H}_{T,1}^L = \bar{H}_T^L$. The excess kurtosis $\lambda_{40} \sim 0.1$ (Bitner-Gregersen et al. 2014; Dias et al. 2015).

8. Concluding remarks

Current freak wave warning systems rely on Janssen's (2003) theory for the kurtosis of surface elevations, a key result with significant implications to the understanding of the role of nonlinear wave interactions in rogue wave formation (Janssen and Bidlot 2009). The present results suggest that in typical oceanic fields third-order quasi-resonant interactions do not appear to play a significant role in the wave growth. Fedele's (2015) refinement of Janssen's theory shows that the large excess kurtosis transient observed during the initial stage of wave evolution is a result of the unrealistic assumption that the initial

wave field is homogeneous and Gaussian. Oceanic wave fields are typically non homogeneous both in space and time, and initial conditions become irrelevant as the wave field tends to a more realistic non-Gaussian nonlinear state where statistics are affected mainly by bound harmonics (Annenkov and Shrira (2013, 2014)). In this regime, statistical predictions of extreme waves can be based on the Tayfun (1980) and Janssen (2009) models to account for both second and third-order nonlinearities. In particular, skewness effects on crest heights are dominant and bound kurtosis must be accounted for to attain more accurate predictions of extremes.

Our statistical analysis of the Andrea storm reveals that space-time extremes cannot explain the actual large Andrea time crest and wave height observed at the measurement point. The ST analysis simply predicts that the mean maximum sea surface height expected over the Ekofisk platform's area is higher than the mean maximum height expected at a fixed point within the same area, irrespective of the significant wave height level. The actual maximum occurs at some point within the area or its boundaries, and the likelihood of that point's coincidence with the point where measurements are done is essentially nil.

Further, both of the time and space-time averages of maxima underestimate the actual Andrea crest and wave heights observed. If one accounts for both second and third-order nonlinearities, the actual crest height nearly coincides with the threshold $h_{1/1000}$ exceeded with probability $1/1000$ by the maximum crest height at a point in a typical 3-hour sea state. This suggests that the Andrea rogue wave is likely to be a rare occurrence in quasi-Gaussian seas. Instead, the actual wave height is not so extreme as the crest height as it nearly coincides with the threshold $H_{1/100}$ exceeded with probability $1/100$ by the maximum wave height at a point. The wave height was not the largest as wave measurements indicate a strong crest-trough asymmetry of the Andrea wave, and according to Boccotti's (2000) QD theory this most likely occurred in the configuration of a maximum crest.

Finally, the present conceptual framework for wave extremes can be applied to higher order resolution wave forecasts and operational models for more accurate predictions of rogue waves.

9. Acknowledgments

FF is grateful to Jean Bidlot for providing the ERA-interim data of the Andrea and Draupner storms and for his support in the data analysis. FF also thanks Michael Banner, Luigi Cavaleri, George Forristall, Aris P. Georgakakos, Peter A. E. M. Janssen, Victor Shrira and M. Aziz Tayfun for discussions on nonlinear wave statistics and random wave fields. Further, FF thanks M. Aziz Tayfun and Philip J. Roberts for revising an early draft of the manuscript, Francesco Barbariol for the support with the

analysis of Acqua Alta measurements and Guillermo Gallego for his support with LaTeX. FF acknowledges partial support from NSF grant CMMI-1068624.

APPENDIX A

Dynamic and Bound Kurtosis

For narrowband waves in deep waters, the evolution of the dynamic excess kurtosis from initial Gaussian conditions is given by (Fedele (2015))

$$C_4^d = BF I^2 J(\tau, R) \quad (A1)$$

where

$$J(\tau; R) = 2 \operatorname{Im} \int_0^\tau \frac{1}{\sqrt{1 - 2i\alpha + 3\alpha^2} \sqrt{1 + 2iR\alpha + 3R^2\alpha^2}} d\alpha. \quad (A2)$$

The maximum is attained at $\tau = \tau_c$ (see Eq. (4)) and given by

$$C_{4,\max}^d(R) = BF I^2 J_p(R), \quad (A3)$$

where

$$\begin{aligned} J_p(R) &= J\left(\frac{1}{\sqrt{3R}}; R\right) \\ &= \operatorname{Im} \int_0^{\frac{1}{\sqrt{3R}}} \frac{2}{\sqrt{1 - 2i\alpha + 3\alpha^2} \sqrt{1 + 2iR\alpha + 3R^2\alpha^2}} d\alpha, \end{aligned}$$

and $\operatorname{Im}(a)$ denotes the imaginary part of a .

Drawing on Janssen and Onorato (2007) and Janssen and Bidlot (2009), the dynamic kurtosis in intermediate waters of depth d is simply computed by replacing the Benjamin-Feir Index with

$$BF I_S^2 = BF I^2 \alpha_S$$

where the depth factor

$$\alpha_S = - \left(\frac{c_g}{c_0} \right)^2 \frac{g X_{nl}}{k_0 \omega_0 \omega_0''},$$

depends on the mean frequency ω_0

$$\omega_0 = \sqrt{gk_0 T_0}, \quad D_0 = \tanh(k_0 d)$$

corresponding to the mean wavenumber k_0 via the linear dispersion relation, the group velocity

$$c_g = \omega_0' = \frac{1}{2} c_0 \left\{ 1 + \frac{2k_0 d}{\sinh(2k_0 d)} \right\}, \quad c_0 = \frac{\omega_0}{k_0},$$

where ω_0' is the first derivative of the angular frequency with respect to the wavenumber k_0 , and the second derivative

$$\omega_0'' = -g \frac{\{D_0 - k_0 d (1 - D_0^2)\}^2 + 4(k_0 d)^2 D_0^2 (1 - D_0^2)}{4\omega_0 k_0 D_0}.$$

Further, the nonlinear interaction coefficient

$$X_{nl} = \frac{9D_0^4 - 10D_0^2 + 9}{8D_0^3} - \frac{1}{k_0 d} \left\{ 1 + \frac{(2c_g - c_0/2)^2}{c_s^2 - c_g^2} \right\},$$

where $c_s = \sqrt{gd}$ is the phase velocity in shallow waters.

The NB bound kurtosis C_4^b is given by Janssen (2009) in the form

$$C_4^b = \lambda_{40}/3 = 8\mu_0^2 (\beta + \gamma + 2(\alpha + \Delta)^2), \quad (\text{A4})$$

where the wave steepness $\mu_0 = k_0 \sigma$,

$$\alpha = \frac{3 - T_0^2}{4T_0^3}, \quad \beta = \frac{3}{64} \frac{8 + (1 - T_0^2)^3}{T_0^6}, \quad \gamma = -\frac{1}{2} \alpha^2,$$

and the wave-induced mean sea level variation

$$\Delta = -\frac{1}{4} \frac{c_s^2}{c_s^2 - c_g^2} \left[2 \frac{1 - T_0^2}{T_0} + \frac{1}{x} \right].$$

In deep waters, $C_4^b = 6\mu_0^2$. Note that Eq. (A4) is not valid for small water depths as second and third-order terms of the associated Stokes expansion can be larger than the linear counterpart (see Eq. (A18) in Janssen (2009)). This implies the constraints $\alpha\mu_m \leq 1$ and $\beta\mu_m/\alpha \leq 1$, which are not violated for the Andrea sea state. Note that further restrictions apply as occurrences of spurious crests on the troughs of large, relatively steep second-order Stokes waves are anomalous and not an inherent characteristic of real waves (Tayfun 2013).

APPENDIX B

Space-Time Statistical Parameters

For space-time extremes, the coefficients in Eq. (14) are given by (Baxevani and Rychlik (2006); Fedele (2012))

$$M_3 = 2\pi \frac{D}{T} \frac{\ell_x}{L_x} \frac{\ell_y}{L_y} \alpha_{xyt},$$

$$M_2 = \sqrt{2\pi} \left(\frac{D}{T} \frac{\ell_x}{L_x} \sqrt{1 - \alpha_{xt}^2} + \frac{D}{T} \frac{\ell_y}{L_y} \sqrt{1 - \alpha_{yt}^2} + \frac{\ell_x}{L_x} \frac{\ell_y}{L_y} \sqrt{1 - \alpha_{xy}^2} \right),$$

$$M_1 = N_D + N_x + N_y,$$

where

$$N_D = \frac{D}{T}, \quad N_x = \frac{\ell_x}{L_x}, \quad N_y = \frac{\ell_y}{L_y}$$

are the average number of waves occurring during the time interval D and along the x and y sides of length ℓ_x and ℓ_y ,

respectively. They all depend on the mean period \bar{T} , mean wavelengths \bar{L}_x and \bar{L}_y in x and y directions:

$$\bar{T} = 2\pi \sqrt{\frac{m_{000}}{m_{002}}}, \quad \bar{L}_x = 2\pi \sqrt{\frac{m_{000}}{m_{200}}}, \quad \bar{L}_y = 2\pi \sqrt{\frac{m_{000}}{m_{020}}}$$

and

$$\alpha_{xyt} = \sqrt{1 - \alpha_{xt}^2 - \alpha_{yt}^2 - \alpha_{xy}^2 + 2\alpha_{xt}\alpha_{yt}\alpha_{xy}}.$$

Here,

$$m_{ijk} = \iint k_x^i k_y^j f^k S(f, \theta) df d\theta$$

are the moments of the directional spectrum $S(f, \theta)$ and

$$\alpha_{xt} = \frac{m_{101}}{\sqrt{m_{200}m_{002}}}, \quad \alpha_{yt} = \frac{m_{011}}{\sqrt{m_{020}m_{002}}}, \quad \alpha_{xy} = \frac{m_{110}}{\sqrt{m_{200}m_{020}}}.$$

APPENDIX C

Threshold h_q exceeded with probability q by the maximum surface height

For 3-D random fields, which are of interest in oceanic applications, the nonlinear probability $P_{\text{FST}}^{(nl)}(\xi; A, D)$ that the maximum surface elevation η_{max} over the area A and during a time interval D exceeds the generic threshold ξH_s is equal to the probability of exceeding the threshold ξ_0 , that is

$$P_{\text{FST}}^{(nl)}(\xi; A, D) = P_{\text{ST}}(\xi_0; A, D) (1 + \Lambda \xi_0^2 (4\xi_0^2 - 1)), \quad (\text{C1})$$

where the Gaussian probability of exceedance (see Eq. 10 and (Adler 1981; Adler and Taylor 2009))

$$P_{\text{ST}}(\xi_0; A, D) = \Pr \{ \eta_{\text{max}} > \xi_0 H_s \} \\ = (16M_3 \xi_0^2 + 4M_2 \xi_0 + M_1) \exp(-8\xi_0^2), \quad (\text{C2})$$

the parameter Λ is given in Eq. 28 and amplitudes ξ and ξ_0 are related by the Tayfun (1980) quadratic equation

$$\xi = \xi_0 + 2\mu \xi_0^2. \quad (\text{C3})$$

The nonlinear threshold $h_q = \xi_q H_s$ exceeded with probability q by η_{max} is given by

$$P_{\text{FST}}^{(nl)}(\xi_q; A, D) = q, \quad (\text{C4})$$

or equivalently

$$P_{\text{ST}}(\xi_{0,q}; A, D) (1 + \Lambda \xi_{0,q}^2 (4\xi_{0,q}^2 - 1)) = q, \quad (\text{C5})$$

where from Eq. (C3)

$$\xi_q = \xi_{0,q} + 2\mu \xi_{0,q}^2. \quad (\text{C6})$$

The mean \bar{h}_q of η_{\max} conditioned on $\eta_{\max} \geq h_q$ then follows by definition from

$$\bar{h}_q/H_s = \frac{\int_{\xi_q}^{\infty} \xi p_{ST}^{(nl)}(\xi; A, D) d\xi}{\int_{\xi_q}^{\infty} p_{ST}^{(nl)}(\xi; A, D) d\xi}, \quad (C7)$$

where the nonlinear pdf

$$p_{FST}^{(nl)}(\xi; A, D) = -\frac{dP_{ST}^{(nl)}}{d\xi}. \quad (C8)$$

Integrating (C7) by parts yields

$$\bar{h}_q/H_s = \frac{\xi_q P_{ST}^{(nl)}(\xi_q) + \int_{\xi_q}^{\infty} P_{ST}^{(nl)}(\xi) d\xi}{P_{ST}^{(nl)}(\xi_q)},$$

and it follows from Eq. (C4) that

$$\bar{h}_q/H_s = \xi_q + \frac{1}{q} \int_{\xi_q}^{\infty} P_{ST}^{(nl)}(\xi) d\xi.$$

Next, note that

$$\int_{\xi_q}^{\infty} P_{FST}^{(nl)}(\xi) d\xi = \int_{\xi_q}^{\infty} P_{ST}(\xi_0) (1 + \Lambda \xi_0^2 (4\xi_0^2 - 1)) d\xi, \quad (C9)$$

where $\xi_0(\xi)$ is a function of the nonlinear ξ given by Eq. (C3). A change of variables via $\xi_0(\xi) = y$ and $d\xi = \frac{d\xi}{d\xi_0} dy = (1 + 4\mu y) dy$ simplify the preceding expression to

$$\int_{\xi_q}^{\infty} P_{ST}^{(nl)}(\xi) d\xi = \int_{\xi_{0,q}}^{\infty} P_{ST}(y) F(y) dy, \quad (C10)$$

where $F(y) = (1 + \Lambda y^2 (4y^2 - 1)) (1 + 4\mu y)$. Further, $\xi_{0,q}$ follows from Eq. (C5) and it relates to ξ_q via Eq. (C6). Therefore,

$$\bar{h}_q/H_s = \xi_q + \frac{1}{q} \int_{\xi_{0,q}}^{\infty} P_{ST}(y) F(y) dy.$$

This expression is written in the form

$$\bar{h}_q = h_q + (\chi_{1,q} + \mu \chi_{2,q} + \Lambda \chi_{3,q} + \mu \Lambda \chi_{4,q}) H_s / q, \quad (C11)$$

where

$$\begin{aligned} \chi_{1,q} &= \int_{\xi_{0,q}}^{\infty} P_{ST}(\xi) d\xi \\ &= p_{1,q} \exp(-8\xi_{0,q}^2) + \frac{\sqrt{2\pi}}{8} (M_1 + M_3) \text{Erfc}(2\sqrt{2}\xi_{0,q}), \\ \chi_{2,q} &= \int_{\xi_{0,q}}^{\infty} 4y P_{ST}(y) dy \\ &= p_{2,q} \exp(-8\xi_{0,q}^2) + \frac{\sqrt{2\pi}}{8} M_2 \text{Erfc}(2\sqrt{2}\xi_{0,q}), \\ \chi_{3,q} &= \int_{\xi_{0,q}}^{\infty} y^2 (4y^2 - 1) P_{ST}(y) dy \\ &= p_{3,q} \exp(-8\xi_{0,q}^2) - \frac{M_1 - 3M_3}{512} \sqrt{2\pi} \text{Erfc}(2\sqrt{2}\xi_{0,q}), \\ \chi_{4,q} &= \int_{\xi_{0,q}}^{\infty} 4y^3 (4y^2 - 1) P_{ST}(y) dy \\ &= p_{4,q} \exp(-8\xi_{0,q}^2) + \frac{3\sqrt{2\pi}}{512} M_2 \text{Erfc}(2\sqrt{2}\xi_{0,q}), \end{aligned}$$

Erfc(x) is the complementary error function and

$$\begin{aligned} p_{1,q} &= \frac{1}{4} (M_2 + 4M_3 \xi_{0,q}), \\ p_{2,q} &= \frac{1}{4} (M_1 + 2M_3 + 4M_2 \xi_{0,q} + 16M_3 \xi_{0,q}^2), \\ p_{3,q} &= \xi_{0,q} \left(\frac{3M_3 - M_1}{64} + \frac{M_1 + M_3}{4} \xi_{0,q}^2 + M_2 \xi_{0,q}^3 + 4M_3 \xi_{0,q}^4 \right), \\ p_{4,q} &= \frac{M_3}{16} + \frac{3M_2}{64} \xi_{0,q} + \frac{M_3}{2} \xi_{0,q}^2 + \frac{M_2}{4} \xi_{0,q}^3 + \\ &\quad (M_1 + 2M_3) \xi_{0,q}^4 + 4M_2 \xi_{0,q}^5 + 16M_3 \xi_{0,q}^6. \end{aligned}$$

References

- Adcock, T., P. Taylor, S. Yan, Q. Ma, and P. Janssen, 2011: Did the draupner wave occur in a crossing sea? *Proceedings of the Royal Society A: Mathematical, Physical and Engineering Science*, rspa20110049.
- Adler, R. J., 1981: *The geometry of random fields*, Vol. 62. Siam.
- Adler, R. J., 2000: On excursion sets, tube formulas and maxima of random fields. *Annals of Applied Probability*, 1–74.
- Adler, R. J., and J. E. Taylor, 2009: *Random fields and geometry*, Vol. 115. Springer Monographs in Mathematics.
- Alber, I. E., 1978: The effects of randomness on the stability of two-dimensional surface wavetrains. *Proceedings of the Royal Society of London A: Mathematical, Physical and Engineering Sciences*, **363 (1715)**, 525–546.
- Ankiewicz, A., N. Devine, and N. Akhmediev, 2009: Are rogue waves robust against perturbations? *Physics Letters A*, **373**, 3997–4000.
- Annenkov, S. Y., and V. I. Shrira, 2009: Evolution of kurtosis for wind waves. *Geophysical Research Letters*, **36 (13)**, 1944–8007, doi:10.1029/2009GL038613, URL <http://dx.doi.org/10.1029/2009GL038613>.

- Annenkov, S. Y., and V. I. Shrira, 2013: Large-time evolution of statistical moments of wind-wave fields. *Journal of Fluid Mechanics*, **726**, 517–546, doi:10.1017/jfm.2013.243, URL <http://journals.cambridge.org/article.S0022112013002437>.
- Annenkov, S. Y., and V. I. Shrira, 2014: Evaluation of skewness and kurtosis of wind waves parameterized by jonswap spectra. *Journal of Physical Oceanography*, **44** (6), 1582–1594, doi:10.1175/JPO-D-13-0218.1, URL <http://dx.doi.org/10.1175/JPO-D-13-0218.1>.
- Barbariol, F., A. Benetazzo, F. Bergamasco, S. Carniel, and M. Sclavo, 2014: Stochastic space–time extremes of wind sea states: Validation and modeling. *ASME 2014 33th International Conference on Ocean, Offshore and Arctic Engineering*, American Society of Mechanical Engineers, OMAE2014–23997.
- Baxevani, A., and I. Rychlik, 2006: Maxima for gaussian seas. *Ocean Engineering*, **33** (7), 895 – 911, doi:<http://dx.doi.org/10.1016/j.oceaneng.2005.06.006>, URL <http://www.sciencedirect.com/science/article/pii/S0029801805001952>.
- Bitner-Gregersen, E. M., L. Fernandez, J. M. Lefèvre, J. Monbaliu, and A. Toffoli, 2014: The north sea andrea storm and numerical simulations. *Natural Hazards and Earth System Science*, **14** (6), 1407–1415, doi:10.5194/nhess-14-1407-2014, URL <http://www.nat-hazards-earth-syst-sci.net/14/1407/2014/>.
- Boccotti, P., 2000: *Wave Mechanics for Ocean Engineering*. Elsevier Sciences, Oxford, 496 pp.
- Chabchoub, A., N. Hoffmann, M. Onorato, and N. Akhmediev, 2012: Super rogue waves: Observation of a higher-order breather in water waves. *Phys. Rev. X*, **2**, 011015, doi:10.1103/PhysRevX.2.011015, URL <http://link.aps.org/doi/10.1103/PhysRevX.2.011015>.
- Chabchoub, A., N. P. Hoffmann, and N. Akhmediev, 2011: Rogue wave observation in a water wave tank. *Phys. Rev. Lett.*, **106**, 204502, doi:10.1103/PhysRevLett.106.204502, URL <http://link.aps.org/doi/10.1103/PhysRevLett.106.204502>.
- Christou, M., and K. Ewans, 2014: Field measurements of rogue water waves. *Journal of Physical Oceanography*, **44** (9), 2317–2335, doi:10.1175/JPO-D-13-0199.1, URL <http://dx.doi.org/10.1175/JPO-D-13-0199.1>.
- Crawford, D. R., B. M. Lake, P. G. Saffman, and H. C. Yuen, 1981: Stability of weakly nonlinear deep-water waves in two and three dimensions. *Journal of Fluid Mechanics*, **105**, 177–191, doi:10.1017/S0022112081003169, URL <http://journals.cambridge.org/article.S0022112081003169>.
- Dee, D. P., and Coauthors, 2011: The era-interim reanalysis: configuration and performance of the data assimilation system. *Quarterly Journal of the Royal Meteorological Society*, **137** (656), 553–597, doi:10.1002/qj.828, URL <http://dx.doi.org/10.1002/qj.828>.
- Dias, F., J. Brennan, S. Ponce de Leon, C. Clancy, and J. Dudley, 2015: Local analysis of wave fields produced from hindcasted rogue wave sea states. *ASME 2015 34th International Conference on Ocean, Offshore and Arctic Engineering*, American Society of Mechanical Engineers, OMAE2015–41458.
- Dyachenko, A. I., and V. E. Zakharov, 2011: Compact Equation for Gravity Waves on Deep Water. *JETP Lett.*, **93** (12), 701–705.
- Dysthe, K. B., H. E. Krogstad, and P. Muller, 2008: Oceanic rogue waves. *Annual Review of Fluid Mechanics*, **40**, 287–310.
- Fedele, F., 2008: Rogue waves in oceanic turbulence. *Physica D*, **237**, 2127–2131.
- Fedele, F., 2012: Space–time extremes in short-crested storm seas. *Journal of Physical Oceanography*, **42** (9), 1601–1615, doi:10.1175/JPO-D-11-0179.1, URL <http://dx.doi.org/10.1175/JPO-D-11-0179.1>.
- Fedele, F., 2014: On certain properties of the compact zakharov equation. *Journal of Fluid Mechanics*, **748**, 692–711, doi:10.1017/jfm.2014.192, URL <http://journals.cambridge.org/article.S002211201400192X>.
- Fedele, F., 2015: On the kurtosis of ocean waves in deep water. *arXiv preprint arXiv:1412.8231*.
- Fedele, F., A. Benetazzo, G. Gallego, P.-C. Shih, A. Yezzi, F. Barbariol, and F. Ardhuin, 2013: Space–time measurements of oceanic sea states. *Ocean Modelling*, **70**, 103–115.
- Fedele, F., Z. Cherneva, M. A. Tayfun, and C. G. Soares, 2010: Non-linear schrodinger invariants and wave statistics. *Physics of Fluids*, **22** (3), 036601, doi:10.1063/1.3325585, URL <http://link.aip.org/link/?PHF/22/036601/1>.
- Fedele, F., and M. A. Tayfun, 2009: On nonlinear wave groups and crest statistics. *J. Fluid Mech.*, **620**, 221–239.
- Forristall, G. Z., 2011: Maximum crest heights under a model tlp deck. *ASME 2011 30th International Conference on Ocean, Offshore and Arctic Engineering*, American Society of Mechanical Engineers, 571–577.
- Forristall, G. Z., 2015: Maximum crest heights over an area: laboratory measurements compared to theory. *ASME 2015 34th International Conference on Ocean, Offshore and Arctic Engineering*, American Society of Mechanical Engineers, OMAE2015–41061.
- Haver, S., 2001: Evidences of the existence of freak waves. *Rogue Waves*, 129–140.
- Haver, S., 2002: On the prediction of extreme wave crest heights. *Proc. of 7th International Workshop on Wave Hindcasting and Forecasting*.
- Haver, S., 2004: A possible freak wave event measured at the draupner jacket january 1 1995. *Proc. of Rogue waves 2004*, 1–8.
- Janssen, P. A. E. M., 2003: Nonlinear four-wave interactions and freak waves. *Journal of Physical Oceanography*, **33** (4), 863–884.
- Janssen, P. A. E. M., 2009: On some consequences of the canonical transformation in the hamiltonian theory of water waves. *Journal of Fluid Mechanics*, **637**, 1–44, doi:10.1017/S0022112009008131, URL <http://journals.cambridge.org/article.S0022112009008131>.
- Janssen, P. A. E. M., 2014: Notes on kurtosis evolution for 2d wave propagation. Memorandum Research Department 60.9/PJ/0387, ECMWF.
- Janssen, P. A. E. M., and J. R. Bidlot, 2009: On the extension of the freak wave warning system and its verification. Tech. Memo 588, ECMWF.
- Janssen, P. A. E. M., and M. Onorato, 2007: The intermediate water depth limit of the zakharov equation and consequences for wave prediction. *Journal of Physical Oceanography*, **37** (10), 2389–2400, doi:10.1175/JPO3128.1, URL <http://dx.doi.org/10.1175/JPO3128.1>.

- Kharif, C., and E. Pelinovsky, 2003: Physical mechanisms of the rogue wave phenomenon. *European Journal of Mechanics - B/Fluids*, **22** (6), 603 – 634, doi:<http://dx.doi.org/10.1016/j.euromechflu.2003.09.002>, URL <http://www.sciencedirect.com/science/article/pii/S0997754603000724>.
- Krasitskii, V. P., 1994: On reduced equations in the Hamiltonian theory of weakly nonlinear surface waves. *J. Fluid Mech.*, **272**, 1–20.
- Longuet-Higgins, M. S., and R. W. Stewart, 1964: Radiation stresses in water waves: a physical discussion, with applications. *Deep-Sea Research*, **11**, 529 – 562.
- Magnusson, K. A., and M. A. Donelan, 2013: The andrea wave characteristics of a measured north sea rogue wave. *Journal of Offshore Mechanics and Arctic Engineering*, **135** (3), 031 108–031 108, URL <http://dx.doi.org/10.1115/1.4023800>.
- Mori, N., and P. A. E. M. Janssen, 2006: On kurtosis and occurrence probability of freak waves. *Journal of Physical Oceanography*, **36** (7), 1471–1483, doi:[10.1175/JPO2922.1](https://doi.org/10.1175/JPO2922.1), URL <http://dx.doi.org/10.1175/JPO2922.1>.
- Mori, N., M. Onorato, and P. A. E. M. Janssen, 2011: On the estimation of the kurtosis in directional sea states for freak wave forecasting. *Journal of Physical Oceanography*, **41** (8), 1484–1497, doi:[10.1175/2011JPO4542.1](https://doi.org/10.1175/2011JPO4542.1), URL <http://dx.doi.org/10.1175/2011JPO4542.1>.
- Onorato, M., D. Proment, and A. Toffoli, 2010: Freak waves in crossing seas. *The European Physical Journal-Special Topics*, **185** (1), 45–55.
- Onorato, M., and Coauthors, 2009: Statistical properties of mechanically generated surface gravity waves: a laboratory experiment in a three-dimensional wave basin. *Journal of Fluid Mechanics*, **627**, 235–257, doi:[10.1017/S002211200900603X](https://doi.org/10.1017/S002211200900603X), URL http://journals.cambridge.org/article_S002211200900603X.
- Osborne, A., 2010: *Nonlinear ocean waves and the inverse scattering transform*, Vol. 97. Elsevier, 917 pp. pp., URL <http://scholar.google.com/scholar?hl=en&btnG=Search&q=intitle:Nonlinear+ocean+waves+and+the+inverse+scattering+transform#1>.
- Osborne, A. R., M. Onorato, and M. Serio, 2000: The nonlinear dynamics of rogue waves and holes in deep-water gravity wave trains. *Phys. Lett. A*, **275** (5-6), 386–393, doi:[10.1016/S0375-9601\(00\)00575-2](https://doi.org/10.1016/S0375-9601(00)00575-2), URL <http://linkinghub.elsevier.com/retrieve/pii/S0375960100005752>.
- Peregrine, D. H., 1983: Water waves, nonlinear Schrödinger equations and their solutions. *Journal of the Australian Mathematical Society Series B*, **25**, 16–43.
- Piterbarg, V. I., 1995: *Asymptotic methods in the theory of Gaussian processes and fields*, Vol. 148. AMS ser. Translations of Mathematical Monographs.
- Ponce de León, S., and C. Guedes Soares, 2014: Extreme wave parameters under north atlantic extratropical cyclones. *Ocean Modelling*, **81** (0), 78 – 88, doi:<http://dx.doi.org/10.1016/j.ocemod.2014.07.005>, URL <http://www.sciencedirect.com/science/article/pii/S146350031400095X>.
- Romolo, A., and F. Arena, 2015: On adler space-time extremes during ocean storms. *Journal of Geophysical Research: Oceans*, n/a–n/a, doi:[10.1002/2015JC010749](https://doi.org/10.1002/2015JC010749), URL <http://dx.doi.org/10.1002/2015JC010749>.
- Rosenthal, W., and S. Lehner, 2008: Rogue waves: Results of the maxwave project. *Journal of Offshore Mechanics and Arctic Engineering*, **130** (2), 021 006–021 006, URL <http://dx.doi.org/10.1115/1.2918126>.
- Sharma, J. N., and R. G. Dean, 1979: *Development and evaluation of a procedure for simulating a random directional second order sea surface and associated wave forces*. 20, University of Delaware.
- Shemer, L., and S. Alperovich, 2013: Peregrine breather revisited. *Physics of Fluids*, **25**, 051 701.
- Shemer, L., and D. Liberzon, 2014: Lagrangian kinematics of steep waves up to the inception of a spilling breaker. *Physics of Fluids*, **26** (1), 016 601, doi:<http://dx.doi.org/10.1063/1.4860235>, URL <http://scitation.aip.org/content/aip/journal/pof2/26/1/10.1063/1.4860235>.
- Shemer, L., and A. Sergeeva, 2009: An experimental study of spatial evolution of statistical parameters in a unidirectional narrow-banded random wavefield. *Journal of Geophysical Research: Oceans*, **114** (C1), 2156–2202, doi:[10.1029/2008JC005077](https://doi.org/10.1029/2008JC005077), URL <http://dx.doi.org/10.1029/2008JC005077>.
- Slunyaev, A., E. Pelinovsky, A. Sergeeva, A. Chabchoub, N. Hoffmann, M. Onorato, and N. Akhmediev, 2013: Super-rogue waves in simulations based on weakly nonlinear and fully nonlinear hydrodynamic equations. *Phys. Rev. E*, **88**, 012 909, doi:[10.1103/PhysRevE.88.012909](https://doi.org/10.1103/PhysRevE.88.012909), URL <http://link.aps.org/doi/10.1103/PhysRevE.88.012909>.
- Slunyaev, A. V., and V. I. Shrira, 2013: On the highest non-breaking wave in a group: fully nonlinear water wave breathers versus weakly nonlinear theory. *Journal of Fluid Mechanics*, **735**, 203–248, doi:[10.1017/jfm.2013.498](https://doi.org/10.1017/jfm.2013.498), URL http://journals.cambridge.org/article_S0022112013004989.
- Socquet-Juglard, H., K. B. Dysthe, K. Trulsen, H. E. Krogstad, and J. Liu, 2005: Probability distributions of surface gravity waves during spectral changes. *Journal of Fluid Mechanics*, **542**, 195–216, doi:[10.1017/S0022112005006312](https://doi.org/10.1017/S0022112005006312), URL http://journals.cambridge.org/article_S0022112005006312.
- Tayfun, M. A., 1980: Narrow-band nonlinear sea waves. *Journal of Geophysical Research: Oceans*, **85** (C3), 1548–1552, doi:[10.1029/JC085iC03p01548](https://doi.org/10.1029/JC085iC03p01548), URL <http://dx.doi.org/10.1029/JC085iC03p01548>.
- Tayfun, M. A., 2006: Statistics of nonlinear wave crests and groups. *Ocean Engineering*, **33** (11–12), 1589 – 1622, doi:<http://dx.doi.org/10.1016/j.oceaneng.2005.10.007>, URL <http://www.sciencedirect.com/science/article/pii/S0029801805002581>.
- Tayfun, M. A., 2008: Distributions of envelope and phase in wind waves. *Journal of Physical Oceanography*, **38** (12), 2784–2800, doi:[10.1175/2008JPO4008.1](https://doi.org/10.1175/2008JPO4008.1), URL <http://dx.doi.org/10.1175/2008JPO4008.1>.
- Tayfun, M. A., 2013: Spurious crests in second-order waves. *Proc. Inter. Conf. on Coastal and Ocean Eng., WASET ICCEO2013*, Zurich, Switzerland.
- Tayfun, M. A., and F. Fedele, 2007: Wave-height distributions and nonlinear effects. *Ocean Engineering*, **34** (11–12), 1631 – 1649, doi:<http://dx.doi.org/10.1016/j.oceaneng.2006.11.006>, URL <http://www.sciencedirect.com/science/article/pii/S0029801807000431>.
- Tayfun, M. A., and J. Lo, 1990: Nonlinear effects on wave envelope and phase. *J. Waterway, Port, Coastal and Ocean Eng.*, **116**, 79–100.

- Toffoli, A., M. Benoit, M. Onorato, and E. M. Bitner-Gregersen, 2009: The effect of third-order nonlinearity on statistical properties of random directional waves in finite depth. *Nonlinear Processes in Geophysics*, **16** (1), 131–139, doi:10.5194/npg-16-131-2009, URL <http://www.nonlin-processes-geophys.net/16/131/2009/>.
- Toffoli, A., O. Gramstad, K. Trulsen, J. Monbaliu, E. Bitner-Gregersen, and M. Onorato, 2010: Evolution of weakly nonlinear random directional waves: laboratory experiments and numerical simulations. *Journal of Fluid Mechanics*, **664**, 313–336, doi: 10.1017/S002211201000385X, URL http://journals.cambridge.org/article_S002211201000385X.
- Walker, D., P. Taylor, and R. E. Taylor, 2004: The shape of large surface waves on the open sea and the draupner new year wave. *Applied Ocean Research*, **26** (3–4), 73 – 83, doi:<http://dx.doi.org/10.1016/j.apor.2005.02.001>, URL <http://www.sciencedirect.com/science/article/pii/S0141118705000052>.